

Photon or meson formation in J/ψ decays into $p\bar{p}$

J.-P. Dedonder

Sorbonne Université, Campus Pierre et Marie Curie, Sorbonne Paris Cité, Université Paris Diderot, et IN2P3-CNRS, UMR 7585, Laboratoire de Physique Nucléaire et de Hautes Énergies, 4 place Jussieu, 75252 Paris, France

B. Loiseau

Sorbonne Université, Campus Pierre et Marie Curie, Sorbonne Paris Cité, Université Paris Diderot, et IN2P3-CNRS, UMR 7585, Laboratoire de Physique Nucléaire et de Hautes Énergies, 4 place Jussieu, 75252 Paris, France

S. Wycech

National Centre for Nuclear Studies, Warsaw, Poland



(Received 2 February 2018; published 21 June 2018)

The measurements of the $J/\psi \rightarrow \gamma p\bar{p}$ decays by the BES Collaboration indicate an enhancement at the $p\bar{p}$ threshold which, however, is not present in the J/ψ decays into $\omega p\bar{p}$ and into $\pi p\bar{p}$. Here, two processes for describing the decays $J/\psi \rightarrow \mathcal{B} p\bar{p}$ where $\mathcal{B} = \gamma, \omega$ are presented in some detail and the cases $\mathcal{B} = \phi, \pi$ are briefly touched on. The first one, applied not only to the radiative decay to reproduce the threshold peak but also to the $\omega p\bar{p}$ decay channel to improve the description of the spectrum, postulates a direct emission of the boson before the baryon pair is formed. The second process assumes that the boson \mathcal{B} is emitted from the baryon pair following the J/ψ decay and includes for the decays into $\gamma p\bar{p}$ a final-state nucleon-antinucleon interaction based on the Paris $N\bar{N}$ potential. The reproduction of the $p\bar{p}$ distribution in the $J/\psi \rightarrow \omega p\bar{p}$ decays needs a final-state interaction involving a $N(2050) 3/2^-$ resonance. The photon- and meson-emission rates are reproduced in a semiquantitative way.

DOI: [10.1103/PhysRevC.97.065206](https://doi.org/10.1103/PhysRevC.97.065206)

I. INTRODUCTION

The J/ψ decays with a proton-antiproton ($p\bar{p}$) pair in the final state are interesting for at least two reasons:

- (1) They are related to the searches for exotic states in the nucleon-antinucleon ($N\bar{N}$) systems. Such searches have been pursued for a few decades, but significant results have been obtained only recently.
- (2) They are closely related to the $p\bar{p}$ reactions, planned at FAIR [1], aiming at the formation of the J/ψ in atomic nuclei.

The first topic is discussed in this paper but the model developed here may be useful to describe the second one. Indication of exotic states below the $N\bar{N}$ threshold may be given by scattering lengths for a given spin and isospin state. However, a clear separation of quantum states in scattering experiments is not easy. Equivalent measurements of the x-ray transitions in the antiproton hydrogen atoms could also select some partial waves if the fine structure of atomic levels is

resolved. So far, only partial selections have been achieved [2]. On the basis of the existing data, the present authors have argued that even averaged fine-structure atomic level widths in the lightest atoms indicate the existence of quasibound $N\bar{N}$ states [3]. Full resolution of the hyperfine structures should be the purpose of future experiments.

To reach specific states, one can also use formation experiments. For instance, in the radiative J/ψ decay,

$$J/\psi \rightarrow \gamma p\bar{p}, \quad (1)$$

an enhancement close to the $p\bar{p}$ threshold has been observed by the BES¹ Collaboration [4,5]. We note that both the J/ψ and the photon have $J^{PC} = 1^{--}$. There are three final $p\bar{p}$ states allowed by parity, P , and charge-conjugation, C , conservations in the $\gamma p\bar{p}$ channel: 1S_0 , 3P_1 , and 3P_0 . Tables I and II indicate the allowed $p\bar{p}$ states, denoted by $^{2S+1}L_J$ or $^{2I+1, 2S+1}L_J$, where S, L, J denote the spin, angular momentum, and total momentum of the pair, respectively, and I indicates the isospin. Two isospin states, $I = 0, 1$, enter the $p\bar{p}$ system. A first indication that the system is in an $I = 0$ state was obtained in a simple quark model in Ref. [6]. In Ref. [7], a unified picture and a limited description of the radiative decays has been achieved in a semiquantitative way. It suggests that the final $\gamma p\bar{p}$ state is dominated by the 1S_0 partial wave.

Published by the American Physical Society under the terms of the Creative Commons Attribution 4.0 International license. Further distribution of this work must maintain attribution to the author(s) and the published article's title, journal citation, and DOI. Funded by SCOAP³.

¹Beijing Electron Spectrometer.

TABLE I. The states of low-energy $p\bar{p}$ pairs allowed in the $J/\psi \rightarrow \gamma p\bar{p}$ and $J/\psi \rightarrow \pi^0 p\bar{p}$ decays. The first column gives decay modes and specifies the internal states of the $p\bar{p}$ pair. Both the J/ψ meson and the photon have $J^{PC} = 1^{--}$. The second column gives J^{PC} for the $p\bar{p}$ system, and the last column gives the relative angular momentum of the photon or pion vs the $p\bar{p}$ pair.

Decay mode	$J^{PC}(p\bar{p})$	Relative l
$\gamma p\bar{p}(^1S_0)$	0^{-+}	1
$\gamma p\bar{p}(^3P_0)$	0^{++}	0
$\gamma p\bar{p}(^3P_1)$	1^{++}	0
$\pi^0 p\bar{p}(^3P_1)$	1^{+-}	0
$\pi^0 p\bar{p}(^3S_1)$	1^{--}	1

In this partial wave, the Paris potential generates a 52-MeV broad quasibound state at 4.8 MeV below threshold [8]. The conclusion that a near-threshold peak is formed in the 1S_0 wave has been reached by the Jülich group, although the Bonn-Jülich potential does not generate a bound state in this wave [9],² and by Chen *et al.* [12] in the framework of an effective $N\bar{N}$ interaction model. Another study of the near-threshold enhancement performed in Ref. [13] finds a quasibound state to be the explanation. The Bonn-Jülich group found recently a good description of the threshold behavior in all mesic channels with a chirally motivated $N\bar{N}$ potential [11]. The conclusion reached is similar to that obtained with the Paris potential: The near-threshold enhancement indicates the presence of a quasibound state.

To understand better the nature of the $p\bar{p}$ states involved, one should look directly into the subthreshold energy region. This may be achieved in the antiproton-deuteron or the antiproton-helium reactions at zero or low energies. Another way to look below the threshold is the detection of $N\bar{N}$ decay products. The specific decay mode

$$J/\psi \rightarrow \gamma \pi^+ \pi^- \eta' \quad (2)$$

has been studied by the BES Collaboration [14]. This reaction is attributed by BES to an intermediate $p\bar{p}$ configuration in the $J^{PC}(p\bar{p}) = 0^{-+}$ state which corresponds to spin singlet S wave. The peak observed in the invariant mass of the mesons has been interpreted as a new baryon state and named $X(1835)$.

Under the assumption that all mesons are produced in relative S waves, reaction (2), if attributed to an intermediate $p\bar{p}$ state, is even more restrictive than reaction (1). It allows only one intermediate state, the $p\bar{p} \ ^1S_0$, which coincides with the previous findings. The intermediate $p\bar{p}$ state in reaction (2)

²For completeness, we want to mention that earlier in Ref. [10] this group had claimed that within a Watson-Migdal approach they could reproduce the near-threshold spectrum with an $l = 1$ state. Also, later in Ref. [11], using for the $N\bar{N}$ interaction a potential derived within chiral effective field theory fitted to results of a partial-wave analysis of $p\bar{p}$ scattering data, the authors claim that the near-threshold spectrum observed in various decay reactions can be reproduced simultaneously and consistently by their treatment of the $p\bar{p}$ fsi and that the interaction in the isospin-1 1S_0 channel, required to fit the decay $J/\psi \rightarrow \gamma p\bar{p}$, predicts an $N\bar{N}$ bound state.

TABLE II. Experimental branching fractions for some decay modes of the J/ψ meson into channels implying $N\bar{N}$ pairs and the corresponding allowed states of the $N\bar{N}$ pair. All data are from Ref. [21] but for the $p\bar{p}\phi$ channel recently measured in Ref. [22].

Decay mode	Experimental branching fractions	$N\bar{N}$ allowed states
$p\bar{p}\pi^0$	$1.19(0.08) \times 10^{-3}$	$^{33}S_1, ^{31}P_1$
$p\bar{p}\pi^-$	$2.12(0.09) \times 10^{-3}$	$^{33}S_1, ^{31}P_1$
$p\bar{p}\gamma$	$3.8(1.0) \times 10^{-4}$	$^1S_0, ^3P_1, ^3P_0$
$p\bar{p}\omega$	$9.8(1.0) \times 10^{-4}$	$^{11}S_0, ^{13}P_1, ^{13}P_0$
$p\bar{p}\phi$	$5.23(0.34) \times 10^{-5}$	$^{11}S_0, ^{13}P_1, ^{13}P_0$
$p\bar{p}$	$2.120(0.029) \times 10^{-3}$	$^{13}S_1$
$n\bar{n}$	$2.09(0.16) \times 10^{-3}$	$^{13}S_1$

is possible but not warranted. In Ref. [15], a more consistent interpretation is obtained with the dominance of the $^{11}S_0$ state which is a mixture of $p\bar{p}$ and $n\bar{n}$ pairs. It has been argued that the peak is due to an interference of a quasibound, isospin-0, $N\bar{N}$ state with a background amplitude. This quasibound state was found by Loiseau and Wycech [7] to be responsible for the threshold enhancement in reaction (1). A recent BES III experiment [16] has studied the radiative decay $J/\psi \rightarrow \gamma \gamma \phi$ and observes a broad bump in the $M(\gamma\phi)$ invariant mass distribution. The shape of this bump is consistent with that observed in the absorptive $N\bar{N}$ amplitude obtained in Ref. [15]. A related strong enhancement of the absorption is observed in the light antiprotonic atoms. The comparison of atomic level widths in a series of atoms ($H, ^2H, ^3H, ^3He, ^4He$) allows us to test the absorption of antiprotons on more strongly bound protons up to subthreshold energies of $E_{p\bar{p}}$ down to -40 MeV [3]. The enhancement of absorption below the $p\bar{p}$ threshold is consistent with both results from Refs. [16] and [3]. This, in our view, provides evidence that the $X(1835)$ meson is due to attraction in the $N\bar{N}$ system.

A similar decay mode

$$J/\psi \rightarrow \pi^0 p\bar{p} \quad (3)$$

displays no near-threshold enhancement [4]. Recent BES III experiments [17,18] have extended these measurements to the reaction

$$J/\psi \rightarrow \omega p\bar{p}. \quad (4)$$

No clear near-threshold enhancement is found although Haidenbauer *et al.* [19] claim the existence of a small signal above phase space very close to this threshold. Beyond, a depression at low $p\bar{p}$ energies is seen in the data. These two reactions indicate a strong P -wave dominance in reaction (3) and a sizable P wave in reaction (4). Both find a natural explanation in the model developed in the present work. Recent experiments find no $p\bar{p}$ threshold structure in the

$$\psi' \rightarrow \gamma p\bar{p} \quad (5)$$

decay [5,20]. This result is puzzling as final $p\bar{p}$ states in this process are the same as the final states in $J/\psi \rightarrow \gamma p\bar{p}$ decay. Within the model discussed here, we find a qualitative explanation for this difference (see Sec. VA).

Different experimental branching fractions for the J/ψ decay modes implying a $p\bar{p}$ pair based on Fermi Laboratory [21] and BES experiments [17,18,21,22] are shown in Table II. One notable fact from this table is that the radiative decay is comparable to the decay into strongly interacting mesons. We will see that this is due to a balance among the phase space (see Appendix A), the coupling constants, strong $N\bar{N}$ interactions, and a direct emission process.

The purpose of the present work is to discuss and correlate the physics of $N\bar{N}$ states produced in the J/ψ decays. The main assumption is that the bosons (photon and mesons) are emitted after the $N\bar{N}$ baryons have been produced. In this way, one obtains branching ratios $\Gamma(N\bar{N}\mathcal{B})/\Gamma(N\bar{N})$ consistent with experimental data for the $\pi^0, \pi^-,$ and ϕ mesons formation, listed in Table II. One free parameter R_0 (the size of initial $N\bar{N}$ source) enters this model and it comes out with a reasonable value of 0.28 fm. On the other hand, to obtain the invariant $p\bar{p}$ mass spectra in the decays and in particular to generate the threshold peak, it is necessary to include an additional mechanism for the photon emission before the baryon formation phase. The peak of interest arises as a result of $p\bar{p}$ final-state interaction in the way described in Refs. [7,9]. The rate of this decay enters as another free parameter.

The content of this paper are as follows. Section II recalls briefly the derivation of the width of the $J/\psi \rightarrow p\bar{p}$ decay mode. Section III develops a model for radiative decay which assumes the photon to be emitted at an early stage of the process. This internal emission model explains the two maxima in the final $p\bar{p}$ spectrum; one is due to baryonium while the other represents a shape resonance in the $p\bar{p}$ interaction. It can be extended to the case of emission of any meson. Section IV discusses the photon or meson (ω, ϕ, π) emission from the final baryon currents, i.e., once the baryons are formed following the decay of the J/ψ . Section V collects the results. In the case of the $J/\psi \rightarrow \omega p\bar{p}$ decay, the description of the $p\bar{p}$ spectrum requires final-state interactions with a $N^*(3/2^-)$ resonance while that of the ωp spectrum requires a contribution of the mechanism of ω emission before the baryon pair formation occurs. A brief summary together with some outlook are given in Sec. VI. Finally, appendixes tackle a number of technical questions.

II. THE $J/\psi \rightarrow p\bar{p}$ AMPLITUDE AND ITS WIDTH

Let the initial J/ψ wave function in momentum space ψ_i be normalized as

$$\psi_i(\mathbf{P}) = \frac{1}{\sqrt{\mathcal{V}_0}} (2\pi)^3 \delta^{(3)}(\mathbf{P}), \quad (6)$$

where \mathcal{V}_0 is the normalization volume. In the rest frame of the J/ψ , the amplitude $A_{N\bar{N}}(\mathbf{q}_1, \mathbf{q}_2)$ that describes the $J/\psi \rightarrow (N\bar{N})_{I=0}$ reaction is given by

$$\begin{aligned} A_{N\bar{N}}(\mathbf{q}_1, \mathbf{q}_2) &= \langle N(\mathbf{q}_1) \bar{N}(\mathbf{q}_2) | \hat{A}_{N\bar{N}} | \psi_i \rangle \\ &= (2\pi)^3 \delta^{(3)}(\mathbf{q}_1 + \mathbf{q}_2) \frac{1}{\sqrt{\mathcal{V}_0}} \mathcal{F}_{J/\psi}(\mathbf{q}_r), \end{aligned} \quad (7)$$

where $\mathcal{F}_{J/\psi}$ denotes the source function associated to the creation of the $N\bar{N}$ pair from the initial J/ψ meson and where \mathbf{q}_1 and \mathbf{q}_2 denote the momenta of the nucleon and the antinucleon respectively. This source function is assumed to

depend only on the relative $N\bar{N}$ momentum \mathbf{q}_r

$$\mathbf{q}_r = \frac{\mathbf{q}_1 - \mathbf{q}_2}{2}. \quad (8)$$

We postulate furthermore the following smooth phenomenological form for the source function

$$\mathcal{F}_{J/\psi}(\mathbf{q}_r) = \mathcal{F}_{J/\psi}(q_r) = F_0 \exp(-q_r^2 R_0^2/2), \quad (9)$$

where R_0 is the radius of the source for the formation of the $N\bar{N}$ pair and F_0 is a normalization constant.

The probability for the $J/\psi \rightarrow p\bar{p}$ decay channel can be written as

$$\begin{aligned} \Gamma(p\bar{p}) &= \frac{1}{2} \int \frac{d\mathbf{q}_1}{(2\pi)^3} \frac{d\mathbf{q}_2}{(2\pi)^3} \frac{\delta(M_{J/\psi} - E(\mathbf{q}_1) - E(\mathbf{q}_2))}{2E(\mathbf{q}_1) 2E(\mathbf{q}_2)} \\ &\quad \times |A_{p\bar{p}}(\mathbf{q}_1, \mathbf{q}_2)|^2, \end{aligned} \quad (10)$$

where we have taken into account the probability to find $p\bar{p}$ in the isospin 0 state, $|\langle I=0 | p\bar{p} \rangle|^2 = 1/2^3$. Using Eq. (7) and the relation $(2\pi)^3 \delta^{(3)}(\mathbf{0}) = \mathcal{V}_0$, one gets

$$\begin{aligned} \Gamma(p\bar{p}) &= \frac{1}{2} \frac{\delta^{(3)}(\mathbf{0})}{\mathcal{V}_0} \int d\mathbf{q} \frac{\delta(M_{J/\psi} - 2E(q))}{[2E(q)]^2} |\mathcal{F}_{J/\psi}(\mathbf{q})|^2 \\ &= \frac{1}{4\pi^2} \int q^2 dq \frac{\delta(M_{J/\psi} - 2E(q))}{[2E(q)]^2} |\mathcal{F}_{J/\psi}(q)|^2 \\ &= \frac{1}{16\pi^2} \frac{q_m}{M_{J/\psi}} |\mathcal{F}_{J/\psi}(q_m)|^2, \end{aligned} \quad (11)$$

where the δ function has provided $q = q_m = \frac{1}{2}\sqrt{M_{J/\psi}^2 - 4m^2}$, where $M_{J/\psi}$ denotes the mass of the J/ψ meson and m is the nucleon mass. This derivation is recalled here to ascertain that the same factors are used for the particle \mathcal{B} formation reactions $J/\psi \rightarrow p\bar{p}\mathcal{B}$. The corresponding decay rates will be referred to the prime $J/\psi \rightarrow p\bar{p}$ rate.

III. DIRECT (INTERNAL) EMISSION AMPLITUDES

The essence of this approach is presented in Fig. 1, where we illustrate the processes at stake in the case of the photon. The photon is emitted before the $p\bar{p}$ pair is formed. It has been shown in Refs. [7] and [9] that this assumption allows us to reproduce the near-threshold enhancement in the $p\bar{p}$ invariant mass ($M_{p\bar{p}}$) distribution. This enhancement is due to the final-state interaction of the two protons. The interactions, Paris potential in Ref. [7] and Bonn-Jülich potential in Ref. [9], are strongly attractive. In the Paris potential case, a quasibound state is generated while none appears in the Bonn potential case. An extension of these calculations to larger values of $M_{p\bar{p}}$ is presented below.

³The isospin structure of the $N\bar{N}$ states, following the convention used in the Paris potential model, is given by $|I=0\rangle = (|p\bar{p}\rangle - |n\bar{n}\rangle)/\sqrt{2}$ and $|I=1\rangle = (|p\bar{p}\rangle + |n\bar{n}\rangle)/\sqrt{2}$, so that one has

$$\langle 0 | p\bar{p} \rangle = \langle 1 | p\bar{p} \rangle = \langle 1 | n\bar{n} \rangle = 1/\sqrt{2} \quad \text{and} \quad \langle 0 | n\bar{n} \rangle = -\langle 0 | p\bar{p} \rangle.$$

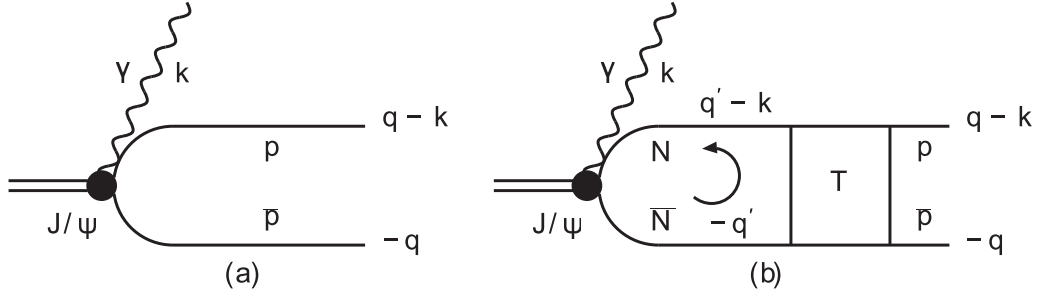


FIG. 1. Photon emission from the J/ψ : the left panel (a) corresponds to the Born term while the right one (b) includes final-state corrections. The nucleon (antinucleon) line is denoted N (\bar{N}) with respective momenta $\mathbf{q}' - \mathbf{k}$ ($-\mathbf{q}'$) while p (\bar{p}) represents a proton (antiproton) propagating with momentum $\mathbf{q} - \mathbf{k}$ ($-\mathbf{q}$). The wavy line is associated to the photon of momentum \mathbf{k} .

In this approach, which will be referred to as the direct emission (DE) model, the direct internal emission process arises either from the charmed $c\bar{c}$ quark pair or from the quark rearrangement stage of the process and its rate is hard to calculate. Here, this rate is fixed by an optimal description of the ratio $\Gamma(p\bar{p}\gamma)/\Gamma(p\bar{p})$ and of the magnitude of the threshold peak. The spectrum is generated by a Born operator, $\widehat{A}_{p\bar{p}\gamma}^{B,DE}$, and final-state interactions (FSI) summed in the operator $\widehat{A}_{p\bar{p}\gamma}^{FSI,DE}$ and collected into the full internal emission operator $\widehat{A}_{p\bar{p}\gamma}^{DE}$ which can be formally written as

$$\begin{aligned} \widehat{A}_{p\bar{p}\gamma}^{DE} &= \widehat{A}_{p\bar{p}\gamma}^{B,DE} + \widehat{A}_{p\bar{p}\gamma}^{FSI,DE} = \widehat{A}_{p\bar{p}\gamma}^{B,DE} [1 + G_{0,N\bar{N}\gamma}^+ T_{[N\bar{N}]}(E_{N\bar{N}})] \\ &= [1 + T_{[N\bar{N}]}(E_{N\bar{N}}) G_{0,N\bar{N}\gamma}^+] \widehat{A}_{p\bar{p}\gamma}^{B,DE}, \end{aligned} \quad (12)$$

where $G_{0,N\bar{N}\gamma}^+$ is the free $N\bar{N}$ propagator at the energy $E_{N\bar{N}}$ in the presence of the photon of momentum \mathbf{k} and $T_{[N\bar{N}]}(E_{N\bar{N}})$ is the $N\bar{N}$ scattering T operator. This operator can act in both $I = 0$ and $I = 1$ states, which occurs for the $N\bar{N}$ pair in the diagram representing the final-state interactions [right panel in Fig. (1)] and will be written when necessary $T_{[N\bar{N}]_I}(E_{N\bar{N}})$. The Born operator $\widehat{A}_{N\bar{N}\gamma}^{B,DE}$ is factorized into two contributions: the $N\bar{N}$ pair creation from the J/ψ meson described through the operator $\widehat{A}_{N\bar{N}}^{J/\psi}$ and the direct photon emission from the J/ψ meson given by the operator \widehat{V}_γ^{DE}

$$\widehat{A}_{N\bar{N}\gamma}^{B,DE} = \widehat{A}_{N\bar{N}}^{J/\psi} \widehat{V}_\gamma^{DE}. \quad (13)$$

The direct photon emission operator \widehat{V}_γ^{DE} has to conserve the charge-conjugation-parity, CP , symmetry. In momentum space, one has three vectors available: \mathbf{k} , $\boldsymbol{\xi}$ (the initial orientation of the J/ψ spin), and the vector product $\boldsymbol{\xi} \wedge \mathbf{k}$ to be combined with the polarization vector of the photon of helicity λ , $\boldsymbol{\epsilon}^*(\lambda)$. The matrix element of the operator \widehat{V}_γ^{DE} associated to a transition to reach a 1S_0 state should then be of the form

$$V_\gamma^{DE}(\mathbf{k}) = g_{DE} \boldsymbol{\epsilon}^*(\lambda) \cdot (\boldsymbol{\xi} \wedge \mathbf{k}), \quad (14)$$

where the constant g_{DE} is a free parameter.

The initial J/ψ meson at rest is described by the momentum space wave function ψ_i given in Eq. (6) and the Born amplitude

$A_{p\bar{p}\gamma}^{B,DE}(\mathbf{q}_r, \mathbf{k})$ is given by the relations

$$\begin{aligned} &\langle p(\mathbf{q}_1) \bar{p}(\mathbf{q}_2) \gamma(\mathbf{k}) | \widehat{A}_{p\bar{p}\gamma}^{B,DE} | \psi_i \rangle \\ &= (2\pi)^3 \delta^{(3)}(\mathbf{q}_1 + \mathbf{q}_2 + \mathbf{k}) A_{p\bar{p}\gamma}^{B,DE}(\mathbf{q}_r, \mathbf{k}), \\ A_{p\bar{p}\gamma}^{B,DE}(\mathbf{q}_r, \mathbf{k}) &= \frac{1}{\sqrt{V_0}} \mathcal{F}_{J/\psi}(\mathbf{q}_r) V_\gamma^{DE}(\mathbf{k}). \end{aligned} \quad (15)$$

The semirelativistic three-particle free $N\bar{N}\gamma$ propagator matrix elements read here

$$\begin{aligned} &\langle \mathbf{q}_1 \mathbf{q}_2 \mathbf{k} | G_{0,N\bar{N}\gamma}^+ | \mathbf{q}'_1 \mathbf{q}'_2 \mathbf{k} \rangle \\ &= (2\pi)^6 \delta^{(3)}(\mathbf{q}_1 - \mathbf{q}'_1) \delta^{(3)}(\mathbf{q}_2 - \mathbf{q}'_2) G_{0,N\bar{N}\gamma}^+(\mathbf{q}_1, \mathbf{q}_2, \mathbf{k}), \end{aligned} \quad (16)$$

where

$$G_{0,N\bar{N}\gamma}^+(\mathbf{q}_1, \mathbf{q}_2, \mathbf{k}) = \frac{1}{E_{N\bar{N}} + i\epsilon - \sqrt{\mathbf{q}_1^2 + m^2} - \sqrt{\mathbf{q}_2^2 + m^2}}, \quad (17)$$

with $E_{N\bar{N}} = M_{J/\psi} - k$ being the $N\bar{N}$ pair energy and $k = |\mathbf{k}|$ being the emitted photon energy. In the evaluation of the final-state interaction contribution, the $N\bar{N}$ pair may be in either isospin $I = 0$ or $I = 1$ state. Thus we may write this contribution as

$$\begin{aligned} &\langle p(\mathbf{q}_1) \bar{p}(\mathbf{q}_2) \gamma(\mathbf{k}) | T_{[N\bar{N}]_I}(E_{N\bar{N}}) G_{0,N\bar{N}\gamma}^+ \widehat{A}_{[N\bar{N}]_I}^{B,DE} | \psi_i \rangle \\ &= \frac{1}{\sqrt{V_0}} \int \langle \mathbf{q}_1 \mathbf{q}_2 | T_{[N\bar{N}]_I}(E_{N\bar{N}}) | \mathbf{q}'_1 \mathbf{q}'_2 \rangle (2\pi)^3 \delta^{(3)} \\ &\quad \times (\mathbf{q}'_1 + \mathbf{q}'_2 + \mathbf{k}) \\ &\quad \times \frac{d\mathbf{q}'_1 d\mathbf{q}'_2}{(2\pi)^6} \frac{1}{E_{N\bar{N}} + i\epsilon - \sqrt{\mathbf{q}'_1^2 + m^2} - \sqrt{\mathbf{q}'_2^2 + m^2}} \\ &\quad \times \mathcal{F}_{J/\psi}(|\mathbf{q}'_r|) V_\gamma^{DE}(\mathbf{k}), \end{aligned} \quad (18)$$

where $\mathbf{q}'_r = (\mathbf{q}'_1 - \mathbf{q}'_2)/2 = \mathbf{q}' - \mathbf{k}/2$ with $\mathbf{q}'_1 = \mathbf{q}' - \mathbf{k}$ and $\mathbf{q}'_2 = -\mathbf{q}'$. Since

$$\begin{aligned} &\langle \mathbf{q}_1 \mathbf{q}_2 | T_{[N\bar{N}]_I}(E_{N\bar{N}}) | \mathbf{q}'_1 \mathbf{q}'_2 \rangle \\ &= (2\pi)^3 \delta^{(3)}(\mathbf{q}'_1 + \mathbf{q}'_2 - \mathbf{q}_1 - \mathbf{q}_2) T_I(\mathbf{q}_r, \mathbf{q}'_r, E_{N\bar{N}}), \end{aligned} \quad (19)$$

we finally arrive at the loop integral that yields the contribution of final-state interactions for the direct photon emission process

$$\begin{aligned} & \langle p(\mathbf{q}_1) \bar{p}(\mathbf{q}_2) \gamma(\mathbf{k}) | T_{[N\bar{N}]}(E_{N\bar{N}}) G_{0,N\bar{N}\gamma}^+ \widehat{A}_{p\bar{p}\gamma}^{B,DE} | \psi_i \rangle \\ & = (2\pi)^3 \delta^{(3)}(\mathbf{q}_1 + \mathbf{q}_2 + \mathbf{k}) A_{p\bar{p}\gamma}^{\text{FSI,DE}}(\mathbf{q}_r, \mathbf{k}, E_{N\bar{N}}), \end{aligned} \quad (20)$$

where

$$\begin{aligned} & A_{p\bar{p}\gamma}^{\text{FSI,DE}}(\mathbf{q}_r, \mathbf{k}, E_{N\bar{N}}) \\ & = \frac{1}{\sqrt{V_0}} V_\gamma^{\text{DE}}(\mathbf{k}) \sum_{I=0,1} \int \frac{d\mathbf{q}'_2}{(2\pi)^3} T_I\left(\mathbf{q}_r, -\mathbf{q}'_2 - \frac{\mathbf{k}}{2}, E_{N\bar{N}}\right) \\ & \times \frac{1}{E_{N\bar{N}} + i\epsilon - \sqrt{(\mathbf{q}'_2 + \mathbf{k})^2 + m^2} - \sqrt{\mathbf{q}'_2{}^2 + m^2}} \\ & \times \mathcal{F}_{J/\psi}\left(\left|\mathbf{q}'_2 + \frac{\mathbf{k}}{2}\right|\right), \end{aligned} \quad (21)$$

\mathbf{q}_r being defined in Eq. (8). Then the full amplitude for the direct photon emission reads

$$\begin{aligned} & \langle p(\mathbf{q}_1), \bar{p}(\mathbf{q}_2), \gamma(\mathbf{k}) | \widehat{A}_{p\bar{p}\gamma}^{\text{DE}} | \psi_i \rangle \\ & = (2\pi)^3 \delta^{(3)}(\mathbf{q}_1 + \mathbf{q}_2 + \mathbf{k}) A_{p\bar{p}\gamma}^{\text{DE}}(\mathbf{q}_r, \mathbf{k}, E_{N\bar{N}}) \\ & = (2\pi)^3 \delta^{(3)}(\mathbf{q}_1 + \mathbf{q}_2 + \mathbf{k}) \left[A_{p\bar{p}\gamma}^{B,DE}(\mathbf{q}_r, \mathbf{k}) \right. \\ & \left. + A_{p\bar{p}\gamma}^{\text{FSI,DE}}(\mathbf{q}_r, \mathbf{k}, E_{N\bar{N}}) \right], \end{aligned} \quad (22)$$

where $A_{p\bar{p}\gamma}^{B,DE}(\mathbf{q}_r, \mathbf{k})$, given by Eq. (15), corresponds to the Born amplitude while the effect of final-state interactions is given by the loop integral $A_{p\bar{p}\gamma}^{\text{FSI,DE}}(\mathbf{q}_r, \mathbf{k}, E_{N\bar{N}})$ of Eq. (21). These results can be similarly extended for the internal emission of a vector meson B where one has simply to replace the potential $V_\gamma^{\text{DE}}(\mathbf{k})$ by an appropriate potential.

The isospin symmetry is violated by the ‘‘internal photon’’ and, as we wrote above in this section, the intermediate state of the baryon pair in Fig. 1(b) is a superposition of $I = 0$ and $I = 1$ $N\bar{N}$ states or of $p\bar{p}$ and $n\bar{n}$ ones. However, the $n\bar{n} \rightarrow p\bar{p}$ transition is weak as the $n\bar{n} \rightarrow p\bar{p}$ cross section is smaller by a factor of the order of 1/15 as compared to the $p\bar{p} \rightarrow p\bar{p}$ cross section; see Ref. [8] for comparison. Hence, in our calculation, the small correction due the $n\bar{n}$ interaction is neglected.

To complete this phenomenological approach, we will assume in addition that, in this process, the source radius has a weak energy dependence on the $p\bar{p}$ invariant mass that reads

$$\begin{aligned} M_{p\bar{p}} & = \sqrt{(M_{J/\psi} - k)^2 - (\mathbf{q}_1 + \mathbf{q}_2)^2} \\ & = \sqrt{M_{J/\psi} (M_{J/\psi} - 2k)}. \end{aligned} \quad (23)$$

We thus write, with masses expressed in units of fm^{-1} ,

$$\begin{aligned} R(M_{p\bar{p}}) & = R_0 + \beta \sqrt{M_{p\bar{p}} - 2m} \\ & = R_0 + \beta \sqrt{M_{J/\psi} \left(1 - \frac{2k}{M_{J/\psi}}\right)^{1/2} - 2m}. \end{aligned} \quad (24)$$

The values $R_0 = 0.28$ fm and $\beta = 0.175 \text{ fm}^{3/2}$ are found to represent the data fairly well. This expression (24) can also be reinterpreted as a modification of the functional form of the source function $\mathcal{F}_{J/\psi}(q_r)$ [see Eq. (9)]. We stay with

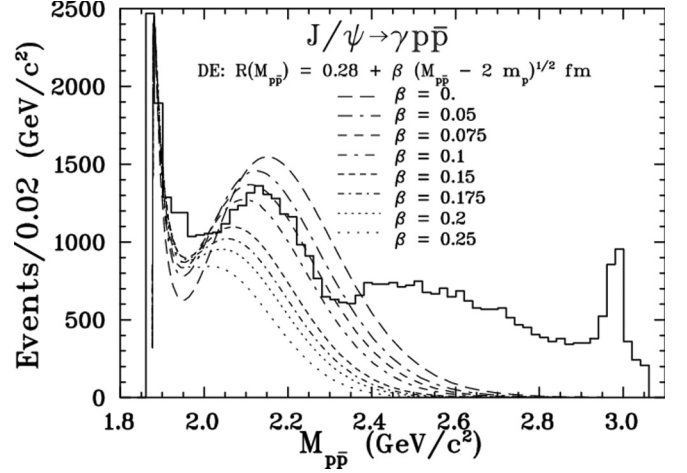


FIG. 2. The invariant $M_{p\bar{p}}$ mass distribution calculated within the direct emission DE model for different values of the parameter β . The data (histogram) is extracted from Fig. 1 in Ref. [5].

this parametrization as it indicates a physical effect indicated below.

By calculating the related loop integral and averaging the probability over the phase space (see Appendixes B and E), one obtains the $M_{p\bar{p}}$ spectrum plotted in Fig. 2 for different values of β . This spectrum has several interesting features summarized in Table III and described below.

- (1) It displays two peaks. The narrow peak that arises at the threshold is related to the near $p\bar{p}$ threshold ($E_{N\bar{N}} = -4.8$ MeV, 52-MeV broad Paris-potential quasibound $^{11}S_0$ state [8]). The other broad peak is formed at $M_{p\bar{p}} \simeq 2130$ MeV. It corresponds to a shape resonance at which the wavelength equals the size of the $p\bar{p}$ potential well in the Paris potential for the $^{11}S_0$ state [8]. The isospin 0 part of the potential well that generates such structures and the corresponding energy-dependent absorptive part are shown in Fig. 3.
- (2) Figure 2 shows the expansion from the initial radius $R_0 = 0.28$ fm to some radius R_f , i.e., when the probability of the photon emission falls to zero and when the $p\bar{p}$ pair is well formed. One sees from the curve on Fig. 2 that the limiting radius R_f varies from 0.28 fm to $R_f \approx 0.61$ fm with the invariant $M_{p\bar{p}}$ mass varying from 2.90 to 2.60 GeV/c^2 when β varies from 0.0 to 0.25 $\text{fm}^{3/2}$.
- (3) The first minimum moves very slowly to slightly increasing invariant $M(p\bar{p})$ mass but remains below the experimental value at about 1.97 GeV/c^2 .
- (4) The broad maximum in the spectrum moves to decreasing values of $M_{p\bar{p}}$ as β increases, i.e., when β goes from 0 to 0.25 $\text{fm}^{3/2}$, the maximum moves from 2.15 to 2.01 GeV/c^2 when the experiment displays a maximum around 2.13 GeV/c^2 . Furthermore, the ratio of the height of the second maximum over the height of the first minimum decreases and goes to 1 as β reaches the value of 0.25 $\text{fm}^{3/2}$; for larger values of β there is neither a minimum nor a maximum.

TABLE III. Position and values of first minimum and second maximum of the direct emission (DE) spectra, all normalized at first maximum value of 2450 events per 0.02 GeV/c².

DE / β in fm ^{3/2}		0	0.05	0.075	0.10	0.15	0.175	0.20	0.25	exp
First min	Position	1.945	1.945	1.955	1.955	1.955	1.9645	1.9645	1.974	1.97
	Height	628	782	834	869	897.7	896.4	883	836	1040
Second max	Position	2.15	2.12	2.11	2.10	2.067	2.058	2.04	2.01	2.13
	Height	1547	1457	1369	1274	1097	1021	953	849	1350
Ratio max/min		2.46	1.86	1.64	1.47	1.22	1.14	1.08	1.02	1.3
Becomes negligible at		2.90	2.85	2.80	2.75	2.70	2.67	2.65	2.60	

We will see further on that the contribution of the baryon current in this process shows a maximum at values of $M_{p\bar{p}}$ slightly above 2.15 GeV.

This internal emission model can be extended to the case of a vector meson emission: The main change comes in the definition of the energy $E_{N\bar{N}}$, i.e., $E_{N\bar{N}} = M_{J/\psi} - \sqrt{m_B^2 + k^2}$, where m_B is the mass of the emitted boson.

IV. BARYON CURRENT AMPLITUDES

This calculation is based on a model suggested in Ref. [7] (similar ideas have been developed quantitatively by Barnes *et al.* in Ref. [23]). The initial assumption is that the mesons are emitted after the $N\bar{N}$ pair has been formed. In the decay process, the initial heavy $c\bar{c}$ quarks in the J/ψ state of $J^{PC} = 1^{--}$ have to disappear and form another $q\bar{q}$ pair. The easiest way to do that is a three-gluon intermediate state [24] which generates a pair of the same J^{PC} . Next, this system generates two extra $q\bar{q}$ pairs from the vacuum, e.g., by the 3P_0 mechanism. This leads to the formation of a 3S_1 state. The emission of γ, π, ϕ , or ω is assumed to happen after the baryons have been formed. It turns out that this assumption yields a generally consistent description of the mesonic decays. Yet, in the case of the γ or ω bosons, it represents only a

sizeable fraction of the decay rate and has to be completed by the contribution of the direct (internal) process just described in the preceding section for the photon case. The mechanism is visualized in Fig. 4 and to quantify it one needs three basic ingredients:

- (1) A wave function to describe the initial $N\bar{N}$ state. It is generated by the $c\bar{c}$ transition to the $^3S_1 N\bar{N}$ state of relative momentum \mathbf{q}_r .
- (2) A mechanism that describes the emission of a boson B from the initial 3S_1 to a final or intermediate $N\bar{N}$ system.
- (3) A method to describe $N\bar{N}$ final-state interactions.

The boson B is emitted with momentum \mathbf{k} from either the nucleon or the antinucleon of final momenta \mathbf{q}_1 and \mathbf{q}_2 , respectively [see Eq. (8)]. The decay amplitude $A_{p\bar{p}B}^{BC}(\mathbf{q}_1, \mathbf{q}_2, \mathbf{k})$ can then be expressed as

$$\begin{aligned}
 A_{p\bar{p}B}^{BC}(\mathbf{q}_1, \mathbf{q}_2, \mathbf{k}) &= \langle p(\mathbf{q}_1) \bar{p}(\mathbf{q}_2) B(\mathbf{k}) | \hat{U}_B G_{0,N\bar{N}}^+ \hat{A}_{N\bar{N}} | \psi_i \rangle \\
 &= \langle p(\mathbf{q}_1) \bar{p}(\mathbf{q}_2) B(\mathbf{k}) | \hat{U}_B | (N\bar{N})_{I=0} \rangle \\
 &\quad \times G_{0,N\bar{N}}^+ \langle (N\bar{N})_{I=0} | \hat{A}_{N\bar{N}} | \psi_i \rangle, \tag{25}
 \end{aligned}$$

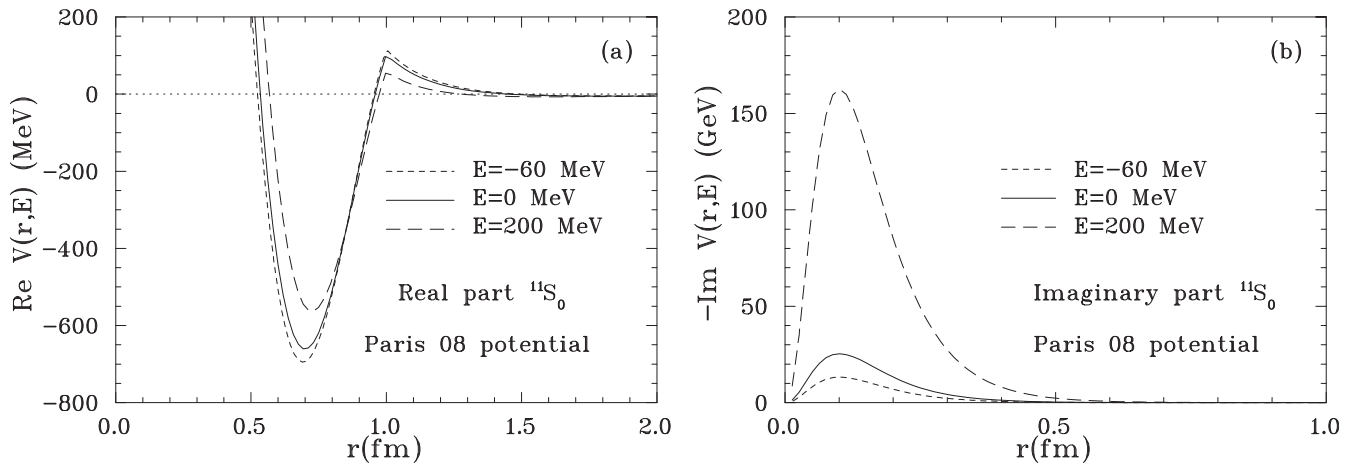


FIG. 3. The left panel (a) displays the real part while the right one (b) displays the absorptive part of the Paris $N\bar{N}$ potential in the isospin 0 isosinglet S wave. The deep well and the barrier are due to the interplay of theoretical one- and two-pion exchange forces supplemented with a short-range phenomenological attraction. The well and barrier structure have the support of 4000 data but the detailed shape of the kink is an artifact of the phenomenological part and it cannot be determined very precisely [8]. The existence of the barrier is nevertheless indicated by the scattering data, in particular those of the $\bar{n}p$ total cross sections.

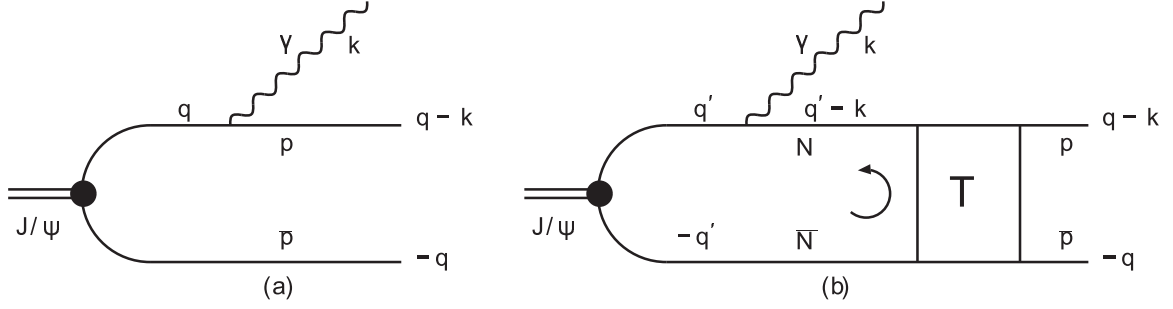


FIG. 4. Photon emission from intermediate baryons: The left graph (a) is associated to the Born term while the right one (b) includes final-state corrections. The various labels have been defined in Fig. 1. Similar diagrams for the emissions from antibaryons are not drawn.

where we assume the initial state to be an $I = 0$ state. We will refer to this as the baryon current (BC) model. The boson emission operator \hat{U}_B includes final state interactions, $G_{0,N\bar{N}}^+$ is the $N\bar{N}$ Green's function before the emission of the boson, and ψ_i is the wave function of the J/ψ meson at rest.

The amplitude in Eq. (25) is built up from three factors: the last one, $\langle (N\bar{N})_{I=0} | \hat{A}_{N\bar{N}} | \psi_i \rangle$, corresponds to the creation of the $N\bar{N}$ pair in an isospin 0 state; the middle one, $G_{0,N\bar{N}}^+$ describes its propagation; while the first one, $\langle p\bar{p}\mathcal{B} | \hat{U}_B | (N\bar{N})_{I=0} \rangle$, describes the emission of the boson of momentum \mathbf{k} , final-state interactions included, and can be written formally as

$$\begin{aligned} & \langle p\bar{p}\mathcal{B} | \hat{U}_B | (N\bar{N})_{I=0} \rangle \\ &= \langle p\bar{p}\mathcal{B} | \hat{U}_B^0 [1 + G_{0,N\bar{N}B}^+ T_{[N\bar{N}]}] | (N\bar{N})_{I=0} \rangle \\ &= \langle p\bar{p}\mathcal{B} | [T_{[N\bar{N}]} G_{0,N\bar{N}B}^+ + 1] \hat{U}_B^0 | (N\bar{N})_{I=0} \rangle, \end{aligned} \quad (26)$$

where $G_{0,N\bar{N}B}^+$ denotes the free three-body Green's function [similar to Eq. (17) in the photon case].

The intermediate $N\bar{N}$ pair being in an isospin $I = 0$ state, the lowest order (Born) amplitude in the absence of final-state interaction (left panel of Fig. 4) is given, since in that case one has only an intermediate $p\bar{p}$ pair, formally by

$$\begin{aligned} & \langle p(\mathbf{q}_1) \bar{p}(\mathbf{q}_2) \mathcal{B}(\mathbf{k}) | \hat{U}_B^0 | (p\bar{p})_{I=0} \rangle G_{0,p\bar{p}}^+ \langle (p\bar{p})_{I=0} | \hat{A}_{p\bar{p}} | \psi_i \rangle \\ &= \int \frac{d\mathbf{q}'_1}{(2\pi)^3} \langle p(\mathbf{q}_1) \bar{p}(\mathbf{q}_2) \mathcal{B}(\mathbf{k}) | \hat{U}_B^0 | [p(\mathbf{q}'_1) \bar{p}(-\mathbf{q}'_1)]_{I=0} \rangle \end{aligned}$$

$$\begin{aligned} & \times \frac{(2\pi)^3}{\sqrt{V_0}} \delta^{(3)}(-\mathbf{q}'_1 + \mathbf{q}_2) \frac{\mathcal{F}_{J/\psi}(q'_1)}{M_{J/\psi} + i\epsilon - 2\sqrt{q\mathbf{q}'_1{}^2 + m^2}} \\ &= (2\pi)^3 \delta^{(3)}(\mathbf{q}_1 + \mathbf{q}_2 + \mathbf{k}) \tilde{A}_{p\bar{p}B}^{B,BC}(\mathbf{q}_2, \mathbf{k}), \end{aligned} \quad (27)$$

where

$$\begin{aligned} & \tilde{A}_{p\bar{p}B}^{B,BC}(\mathbf{q}_2, \mathbf{k}) = \tilde{G}_{p\bar{p}}(q_2) U_{p\bar{p}B}^0(\mathbf{q}_2, \mathbf{k}) \quad \text{with} \\ & \tilde{G}_{p\bar{p}}(q_2) = \frac{1}{\sqrt{V_0}} \frac{\mathcal{F}_{J/\psi}(q_2)}{M_{J/\psi} + i\epsilon - 2\sqrt{q\mathbf{q}_2{}^2 + m^2}}. \end{aligned} \quad (28)$$

In these equations, the photon (meson) is emitted from the nucleon of momentum \mathbf{q}_1 and the antinucleon is the spectator with momentum \mathbf{q}_2 such that $\mathbf{q}_2 = -\mathbf{q}$, $\mathbf{q}_1 = -\mathbf{q}_2 - \mathbf{k} = \mathbf{q} - \mathbf{k}$ and $\mathbf{q}_r = \mathbf{q} - \mathbf{k}/2$.

The FSI contribution contains the formal expression

$$\begin{aligned} & \langle p\bar{p}\mathcal{B} | T_{N\bar{N}} G_{0,N\bar{N}B}^+ \hat{U}_B^0 | (N\bar{N})_{I=0} \rangle \\ &= \sum_I \langle p\bar{p}\mathcal{B} | (N\bar{N})_I \rangle \langle (N\bar{N})_I | T_{[N\bar{N}]} \rangle \\ & \times G_{0,N\bar{N}B}^+ | (N\bar{N})_I \rangle \langle (N\bar{N})_I | \hat{U}_B^0 | (N\bar{N})_{I=0} \rangle \end{aligned} \quad (29)$$

where the sum over the isospin I is restricted to $I = 0, 1$. We may then write explicitly

$$\begin{aligned} & A_{p\bar{p}B}^{\text{FSL,BC}}(\mathbf{q}_1, \mathbf{q}_2, \mathbf{k}) = \langle p(\mathbf{q}_1) \bar{p}(\mathbf{q}_2) \mathcal{B}(\mathbf{k}) | T_{N\bar{N}} G_{0,N\bar{N}B}^+ \hat{U}_B^0 | (N\bar{N})_{I=0} \rangle G_{0,N\bar{N}}^+ \langle (N\bar{N})_{I=0} | \hat{A}_{N\bar{N}} | \psi_i \rangle \\ &= \sum_{I=0,1} \int \langle p(\mathbf{q}_1) \bar{p}(\mathbf{q}_2) \mathcal{B}(\mathbf{k}) | T_{[N\bar{N}]} G_{0,N\bar{N}B}^+ | [N(\mathbf{q}'_1) \bar{N}(\mathbf{q}'_2)]_I \mathcal{B}(\mathbf{k}') \rangle \frac{d\mathbf{q}'_1}{(2\pi)^3} \frac{d\mathbf{q}'_2}{(2\pi)^3} \frac{d\mathbf{k}'}{(2\pi)^3} \\ & \times \langle [N(\mathbf{q}'_1) \bar{N}(\mathbf{q}'_2)]_I \mathcal{B}(\mathbf{k}') | \hat{U}_B^0 | (N\bar{N})_{I=0} \rangle G_{0,N\bar{N}}^+ \langle (N\bar{N})_{I=0} | \hat{A}_{N\bar{N}} | \psi_i \rangle \\ &= \sum_{I=0,1} \int \langle p(\mathbf{q}_1) \bar{p}(\mathbf{q}_2) \mathcal{B}(\mathbf{k}) | T_{[N\bar{N}]} | [N(\mathbf{q}'_1) \bar{N}(\mathbf{q}'_2)]_I \rangle G_{0,N\bar{N}B}^+(\mathbf{q}'_1, \mathbf{q}'_2, \mathbf{k}) \\ & \times \frac{d\mathbf{q}'_1}{(2\pi)^3} \frac{d\mathbf{q}'_2}{(2\pi)^3} (2\pi)^3 \delta^{(3)}(\mathbf{q}'_1 + \mathbf{q}'_2 + \mathbf{k}) A_{N\bar{N}B}^{B,BC}(\mathbf{q}'_2, \mathbf{k}). \end{aligned} \quad (30)$$

Then, from Eqs. (19), (27), and (28), we obtain

$$A_{p\bar{p}B}^{\text{FSI,BC}}(\mathbf{q}_1, \mathbf{q}_2, \mathbf{k}) = (2\pi)^3 \delta^{(3)}(\mathbf{q}_1 + \mathbf{q}_2 + \mathbf{k}) \tilde{A}_{p\bar{p}B}^{\text{FSI,BC}}(\mathbf{q}_r, \mathbf{k}),$$

$$\tilde{A}_{p\bar{p}B}^{\text{FSI,BC}}(\mathbf{q}_r, \mathbf{k}) = \sum_I \int \frac{d\mathbf{q}'_2}{(2\pi)^3} T_I(\mathbf{q}_r, -\mathbf{q}'_2 - \frac{\mathbf{k}}{2}, E_{N\bar{N}}) G_{0,N\bar{N}B}^+(-\mathbf{q}'_2 - \mathbf{k}, \mathbf{q}'_2, \mathbf{k}) A_{N\bar{N}B}^{B,BC}(\mathbf{q}'_2, \mathbf{k}), \quad (31)$$

where

$$G_{0,N\bar{N}B}^+(-\mathbf{q}'_2 - \mathbf{k}, \mathbf{q}'_2, \mathbf{k}) = \frac{1}{M_{J/\psi} + i\epsilon - E_B(k) - \sqrt{(\mathbf{q}'_2 + \mathbf{k})^2 + m^2} - \sqrt{\mathbf{q}'_2^2 + m^2}}, \quad (32)$$

with $E_B(k) = \sqrt{k^2 + m_B^2}$. The FSI amplitude (31) requires integrations over the corresponding loop momenta and its detailed form will be discussed in the appendixes. Finally, the amplitude in the BC + FSI model is given by

$$A_{p\bar{p}B}^{\text{BC}}(\mathbf{q}_1, \mathbf{q}_2, \mathbf{k}) = (2\pi)^3 \delta^{(3)}(\mathbf{q}_1 + \mathbf{q}_2 + \mathbf{k}) [\tilde{A}_{p\bar{p}B}^{B,BC}(\mathbf{q}_r, \mathbf{k}) + \tilde{A}_{p\bar{p}B}^{\text{FSI,BC}}(\mathbf{q}_r, \mathbf{k})], \quad (33)$$

with $\tilde{A}_{p\bar{p}B}^{B,BC}(\mathbf{q}_r, \mathbf{k})$ given by Eq. (28) and $\tilde{A}_{p\bar{p}B}^{\text{FSI,BC}}(\mathbf{q}_r, \mathbf{k})$ by Eq. (31). One has to add a similar contribution for the emission from the antinucleon. This specific final-state interaction correction will be evaluated with the half off-shell scattering matrix [15] arising from the Paris potential [8]. It will be applied in what follows to the cases of the photon and of the ω meson. The explicit expression of the amplitude for the photon emission is calculated in Appendix C 1. The lowest order amplitude is enhanced by the $N\bar{N}$ final-state interactions and the effect is significant in the spin singlet S wave. As indicated by the summation over the isospin I states, it involves also radiation of magnetic photons from the intermediate $N\bar{N}$ pairs and generates a delicate interference pattern. Since the intermediate states involve $I = 0$, this amplitude is expected to determine, or contribute significantly, to the shape of the threshold peak in the invariant $p\bar{p}$ mass distribution.

A. The initial $N\bar{N}$ state

In the two models describing the $p\bar{p}$ threshold peak [7,9], it was assumed that in the course of radiative process the $p\bar{p}$ final state is formed in the spin singlet 1S_0 state [15]. The near-threshold enhancement arises as a result of the $I = 0$, $p\bar{p}$ final-state interaction. However, in order to understand the full energy spectrum and mesonic emission rates, one needs a better description of the formation mechanism. We go one step further; in addition to the state indicated above, the initial $N\bar{N}$ state is assumed to inherit the spin and isospin quantum numbers of the J/ψ , $S = 1$, $I = 0$, and hence it is a 3S_1 state.

Before the emission of the photon, the process is given by the matrix element:

$$\langle [N(\mathbf{q}_1)\bar{N}(\mathbf{q}_2)]_{I=0} | G_{0,N\bar{N}}^+ \hat{A}_{N\bar{N}} | \psi_i \rangle = (2\pi)^3 \delta^{(3)}(\mathbf{q}_1 + \mathbf{q}_2) \tilde{G}_{N\bar{N}}(q_2), \quad (34)$$

where $\tilde{G}_{N\bar{N}}(q_2)$ is given by Eq. (28) with, in the J/ψ rest frame, $\mathbf{q}_1 = -\mathbf{q}_2 = \mathbf{q}_r = \mathbf{q}$. This free Green's function becomes singular when the momentum approaches its on-shell value. This singularity leads, in the case of electric photon emissions, to

the well-known infrared catastrophe. The effect of infrared enhancement should be seen in the experimental data as a peak at the end of the spectrum, that is, in the soft photon limit. However, it is also clear [4,5] that contributions from the infrared photons ($k < 50$ MeV/c) have been effectively cut out from the data. We refer the reader to the discussion at the end of Sec. V A.

B. The emission vertices

The electromagnetic current associated to the photon emission from the nucleon is given by

$$\langle q' | J_\nu | q \rangle = e \bar{u}(q') \left[\gamma_\nu + \frac{\kappa}{2im} \sigma_{\mu\nu} (q' - q)^\mu \right] u(q)$$

$$= e \bar{u}(q') \left[\gamma_\nu + i \frac{\kappa}{2m} \sigma_{\mu\nu} k^\mu \right] u(q), \quad (35)$$

where

$$\sigma_{\mu\nu} = \frac{i}{2} [\gamma_\mu, \gamma_\nu],$$

e is the unit of charge and κ is the anomalous magnetic moment of the nucleon ($\kappa_p = 1.793$ for the proton and $\kappa_n = -1.913$ for the neutron). The final nucleon four-momentum q' is related to the initial four-momentum q by $q' = q - k$ where k is the emitted boson four-momentum. The corresponding current for the photon emission from the antinucleon will be given by the substitution $e \rightarrow -e$ and $\mathbf{q} \rightarrow -\mathbf{q}$.

More generally, the emission of a vector particle by a nucleon is described by the operator

$$L = g_V \gamma_\nu \epsilon^{\nu*}(\lambda) + i \frac{g_T}{2m} \sigma_{\mu\nu} k^\mu \epsilon^{\nu*}(\lambda), \quad (36)$$

where the four-vector $\epsilon^*(\lambda)$ denotes the polarization vector of the emitted particle, λ is its helicity, while g_V and $g_T = \kappa g_V$ are the vector and tensor coupling constants, respectively.

The final photon or vector meson may be produced in a magnetic or an electric transition. The relevant formation amplitudes are obtained from the transition matrix elements of the operator (36) reducing bispinors u to spinors χ_S . We have

$$\bar{u}(q') L u(q) = \chi_{S'}^\dagger \hat{U}_B^0 \chi_S, \quad (37)$$

where S and S' denote the initial and final nucleon spin, and one obtains the vertex coupling in the two-dimensional spin space

$$\hat{U}_B^0 = g_V \hat{A}_V + i \frac{g_T}{2m} \hat{A}_T. \quad (38)$$

The explicit expressions for the vector \widehat{A}_V and the tensor \widehat{A}_T parts are derived in Appendix C [see Eqs. (C11) and (C17), respectively].

1. The photon case

The full photon potential operator, $U_\gamma^0(\mathbf{k}, \mathbf{q})$, combining the photon emission from either baryon, is given by Eqs. (C22) and (C23). The magnetic terms in $U_\gamma^0(\mathbf{k}, \mathbf{q})$, proportional to $\boldsymbol{\sigma} \cdot [\mathbf{k} \wedge \boldsymbol{\epsilon}^*(\lambda)]$, change the 3S_1 state of the initial $N\bar{N}$ system to the final 1S_0 state. Electric terms in $U_\gamma^0(\mathbf{k}, \mathbf{q})$ proportional to $\mathbf{q} \cdot \boldsymbol{\epsilon}^*(\lambda)$, change the 3S_1 state to final 3P states. Relativistic corrections generate additional terms, most of these cancel in the $p\bar{p}$ system, some spin operators bilinear in \mathbf{q} lead to D waves but contribute corrections only on 1% level and are not included in the calculations. As discussed in Appendix C, the two basic couplings add coherently for the proton and the antiproton. Thus, the summary coupling of photons to the $p\bar{p}$ system becomes

$$U_\gamma^0(\mathbf{q}, \mathbf{k}) = V_{E,\gamma} + V_{M,\gamma} \quad (39)$$

with

$$V_{E,\gamma} = \frac{e}{2m} [C_E \mathbf{q} \cdot \boldsymbol{\epsilon}^*(\lambda)], \quad (40)$$

$$V_{M,\gamma} = i \frac{e}{2m} \{ \mathbf{C}_M \cdot [\mathbf{k} \wedge \boldsymbol{\epsilon}^*(\lambda)] \}, \quad (41)$$

which are still operators in the spin-isospin space and where [see Eqs. (D14) and (D19)]

$$\begin{aligned} C_E &= - \left\{ \zeta + \bar{\zeta} + \frac{1}{\zeta} + \frac{1}{\bar{\zeta}} \right\} + \kappa \frac{k}{2m} \left\{ \zeta + \bar{\zeta} - \frac{1}{\zeta} - \frac{1}{\bar{\zeta}} \right\} \\ &\quad + \kappa \frac{k^2}{2m\Omega} \left\{ \frac{1}{\zeta} + \frac{1}{\bar{\zeta}} \right\}, \\ \mathbf{C}_M &= r_- (\boldsymbol{\sigma}_1 - \boldsymbol{\sigma}_2) + r_+ (\boldsymbol{\sigma}_1 + \boldsymbol{\sigma}_2), \end{aligned} \quad (42)$$

with

$$\begin{aligned} r_- &= \frac{1}{2} \left\{ \left(\frac{1}{\zeta} + \frac{1}{\bar{\zeta}} \right) \left(1 + \kappa \frac{k}{2m} \right) + \kappa \frac{\Omega}{2m} (\zeta + \bar{\zeta}) \right\}, \\ r_+ &= \frac{1}{2} \left\{ \left(\frac{1}{\zeta} - \frac{1}{\bar{\zeta}} \right) \left(1 + \kappa \frac{k}{2m} \right) + \kappa \frac{\Omega}{2m} (\zeta - \bar{\zeta}) \right\}. \end{aligned} \quad (43)$$

The energies Ω, Ω' and the coefficients $\zeta, \bar{\zeta}$ are defined in Appendix C [Eqs. (C6), (C9), and (C13)]. The approximation leading to Eqs. (40)–(43) may be acceptable close to the central region of the $M_{p\bar{p}}$ distribution (see Fig. 6). It is too crude in the threshold region where $k/m \approx 1$ and at the other extremity where $q/m \approx 1$. Nevertheless, some coefficients in $U_\gamma^0(\mathbf{k}, \mathbf{q})$ [Eqs. (C22) and (C23)] display remarkable stability. This, in particular, concerns the terms $\zeta + \bar{\zeta}, \zeta + 1/\zeta, \bar{\zeta} + 1/\bar{\zeta}, \bar{\zeta} + 1/\bar{\zeta}$ which are approximately 2 within 1% over all the phase space. On the other hand, there are a number of terms involving more complicated combinations of the spin and momenta which are less stable, but small due to other reasons. The

terms

$$\frac{ie}{2m} \frac{\kappa}{2m\Omega} \left[\left(\frac{\boldsymbol{\sigma}_1}{\zeta} - \frac{\boldsymbol{\sigma}_2}{\bar{\zeta}} \right) \cdot (\mathbf{k} \wedge \mathbf{q}) \right] [\mathbf{q} \cdot \boldsymbol{\epsilon}^*(\lambda)],$$

$$\frac{ie}{2m} \frac{\kappa}{2m\Omega} \mathbf{q} \cdot \mathbf{k} \left\{ \frac{\boldsymbol{\sigma}_1}{\zeta} - \frac{\boldsymbol{\sigma}_2}{\bar{\zeta}} \right\} \cdot [\mathbf{q} \wedge \boldsymbol{\epsilon}^*(\lambda)],$$

and

$$\frac{ie}{2m} \frac{\kappa}{2m\Omega} \mathbf{q} \cdot [\mathbf{k} \wedge \boldsymbol{\epsilon}^*(\lambda)] \left(\frac{\boldsymbol{\sigma}_1}{\zeta} - \frac{\boldsymbol{\sigma}_2}{\bar{\zeta}} \right) \cdot \mathbf{q},$$

involve a spin flip transition. According to CP conservation (see Table I), these terms lead predominantly to final spin singlet S -wave state. The resulting contribution would give an average $\langle q_i q_j \rangle = q^2/3$ and would mainly contribute at large k , i.e., in the threshold region where corrections will be of the order of $q^2/12m^2$, i.e., about 2%. The term proportional to $\mathbf{q} \wedge \boldsymbol{\epsilon}^*(\lambda)$ in Eq. (C22) reads

$$\begin{aligned} [g(\mathbf{q}, \mathbf{k}) \boldsymbol{\sigma}_1 + \bar{g}(\mathbf{q}, \mathbf{k}) \boldsymbol{\sigma}_2] &= [\tilde{r}_- (\boldsymbol{\sigma}_1 - \boldsymbol{\sigma}_2) + \tilde{r}_+ (\boldsymbol{\sigma}_1 + \boldsymbol{\sigma}_2)] \\ &= 2 (\tilde{r}_- \boldsymbol{\sigma}_- + \tilde{r}_+ \boldsymbol{\sigma}_+), \end{aligned} \quad (44)$$

with

$$\begin{aligned} \tilde{r}_- &= \frac{1}{2} \left\{ (\zeta - \bar{\zeta}) \left(1 - \kappa \frac{k_0}{2m} \right) - \left(\frac{1}{\zeta} - \frac{1}{\bar{\zeta}} \right) \right. \\ &\quad \left. \times \left(1 + \kappa \frac{k_0}{2m} \right) \left(1 + \frac{k_0}{\Omega} \right) \right\}, \\ \tilde{r}_+ &= \frac{1}{2} \left\{ (\zeta + \bar{\zeta}) \left(1 - \kappa \frac{k_0}{2m} \right) - \left(\frac{1}{\zeta} + \frac{1}{\bar{\zeta}} \right) \right. \\ &\quad \left. \times \left(1 + \kappa \frac{k_0}{2m} \right) \left(1 + \frac{k_0}{\Omega} \right) \right\}. \end{aligned} \quad (45)$$

It involves a dominant $\boldsymbol{\sigma}_+ \cdot [\mathbf{q} \wedge \boldsymbol{\epsilon}^*(\lambda)]$ combination which generates spin triplet P -wave states. It could be contributing as much as 20% of the dominant electric term. However, it is only important close to the threshold region where

$$\tilde{r}_+ \approx - \frac{k_0}{\Omega} \left[1 + \kappa \frac{\Omega}{m} \left(1 + \frac{k_0}{2\Omega} \right) \right], \quad (46)$$

but where the P -wave contributions are strongly suppressed by the phase space.

In practical calculations, it is sufficient to neglect small corrections of the order of $k^2/4m^2$ which contribute about 3% to the electric rate, and about 1% to the total rate. On the other hand, a sizable, i.e., of the order of 10%, relativistic correction is due to the $\kappa/2m$ term affecting the anomalous magnetic moment in Eq. (43). Note that in the limit $k/2m \ll 1$, to order, $k^2/4m^2$, Eq. (39) reduces to the simple expression

$$\begin{aligned} U_\gamma^0(\mathbf{q}, \mathbf{k}) &\approx \frac{e}{2m} \left\{ -4 \mathbf{q} \cdot \boldsymbol{\epsilon}^*(\lambda) + i \left(1 + \frac{\kappa\Omega}{2m} \right) (\boldsymbol{\sigma}_1 - \boldsymbol{\sigma}_2) \right. \\ &\quad \left. \cdot [\mathbf{k} \wedge \boldsymbol{\epsilon}^*(\lambda)] \right\}. \end{aligned} \quad (47)$$

2. The vector meson case

The emitted ω meson has a negative G parity and couplings to the proton or the antiproton differ in sign (this also applies

to the case of the π meson emission). Again the emission by a baryon or an antibaryon is predominantly coherent as this sign is compensated by the momentum and/or spin involved in the vertices. In the case of the ω meson, the tensor coupling is known to be consistent with zero and the main contribution comes from the vector coupling [25]. From Eqs. (C25), one infers that the first $\epsilon_0^*(\lambda) = \mathbf{k} \cdot \boldsymbol{\epsilon}^*(\lambda)/k_0$ term [Eq. (C3)] almost disappears, by the G -parity rule, when the emissions from nucleon and antinucleon are added. By retaining only the dominant pieces in Eq. (C26), that is, neglecting terms of the order of $k^2/2\Omega E_q$ or $k^2/4m^2$, one obtains, with k_0 defined in Eq. (C24) and E_q in Eq. (C7),

$$U_\omega^0(\mathbf{q}, \mathbf{k}) \approx -\frac{g_{V\omega}}{2m} \left[4 \mathbf{q} \cdot \boldsymbol{\epsilon}^*(\lambda) + 2 \frac{\mathbf{k} \cdot \mathbf{q}}{E_q} \frac{\mathbf{k} \cdot \boldsymbol{\epsilon}^*(\lambda)}{k_0} - i(\boldsymbol{\sigma}_1 - \boldsymbol{\sigma}_2) \cdot \{\mathbf{k} \wedge \boldsymbol{\epsilon}^*(\lambda)\} \right], \quad (48)$$

which implies that one neglects the following contributions:

$$-i \frac{g_{V\omega}}{2m\Omega} \left[\frac{\mathbf{k} \cdot \mathbf{q}}{E_q} \{(\boldsymbol{\sigma}_1 - \boldsymbol{\sigma}_2) \cdot [\mathbf{q} \wedge \boldsymbol{\epsilon}^*(\lambda)]\} + \frac{\mathbf{k} \cdot \boldsymbol{\epsilon}^*(\lambda)}{k_0} \{(\boldsymbol{\sigma}_1 + \boldsymbol{\sigma}_2) \cdot (\mathbf{k} \wedge \mathbf{q})\} \right] \quad (49)$$

in addition to a term that disappears since it contains the expression

$$1 - 2 \frac{E_q}{\Omega} + \frac{q^2}{\Omega^2} = 0.$$

The first term in Eq. (49)

$$i \frac{g_{V\omega}}{2m\Omega} \frac{\mathbf{k} \cdot \mathbf{q}}{E_q} [(\boldsymbol{\sigma}_1 - \boldsymbol{\sigma}_2) \cdot \{\mathbf{q} \wedge \boldsymbol{\epsilon}^*(\lambda)\}]$$

has to be compared to the basic magnetic contribution

$$i \frac{g_{V\omega}}{2m} [(\boldsymbol{\sigma}_1 - \boldsymbol{\sigma}_2) \cdot \{\mathbf{k} \wedge \boldsymbol{\epsilon}^*(\lambda)\}],$$

since they both lead to S -wave magnetic transitions. For average momenta of the order of 500 MeV/c, the neglected term is of the order of 0.1 of the dominant one. Taking into account the interference contribution in the probability reduces further this contribution, justifying its neglect.

The second term in Eq. (49)

$$i \frac{g_{V\omega}}{2m\Omega} \frac{\mathbf{k} \cdot \boldsymbol{\epsilon}^*(\lambda)}{k_0} \{(\boldsymbol{\sigma}_1 + \boldsymbol{\sigma}_2) \cdot (\mathbf{k} \wedge \mathbf{q})\},$$

which gives rise to 3P waves, has to be compared to the basic electric contribution

$$-4 \frac{g_{V\omega}}{2m} \mathbf{q} \cdot \boldsymbol{\epsilon}^*(\lambda),$$

and, in the absence of any interference contribution, leads to a very small contribution on the order of 10^{-3} of the basic decay rate.

Apart from the magnitude of the coupling constant, there is one important difference with respect to the photon. The magnetic coupling is weak in comparison to the electric one. The reverse was true in the γ case due to the large

proton magnetic moment. This is the basic reason making the transition to the final 1S_0 state small (about 1/10 of the total).

3. The pion case

For π mesons, we use the standard γ_5 coupling

$$U_\pi^0(\mathbf{q}, \mathbf{k}) \approx g_\pi \boldsymbol{\sigma} \cdot \left[\frac{\mathbf{q} - \mathbf{k}}{E_{\mathbf{q}-\mathbf{k}} + m} - \frac{\mathbf{q}}{E_{\mathbf{q}} + m} \right] \boldsymbol{\tau} \cdot \boldsymbol{\varphi}_\pi \simeq -\frac{g_\pi}{2m} (\boldsymbol{\sigma} \cdot \mathbf{k}) (\boldsymbol{\tau} \cdot \boldsymbol{\varphi}_\pi). \quad (50)$$

In this case, the emission requires a spin flip and a change of nucleon angular momentum leading to the final $p\bar{p}$ in the $^3^1P_1$ state. This mechanism eliminates the possibility of 1S_0 states and does not produce any threshold enhancement as indicated by the BES experiments [4,5,17,18].

C. The $N\bar{N}$ final-state interactions

The emission of a magnetic photon from the nucleon in the reaction

$$J/\psi \rightarrow \gamma p\bar{p} \quad (51)$$

generates, within our model, the final spin-0 state in the $p\bar{p}$ system. The corresponding operator in spin space is denoted, in the small $k/2m$ limit and up to the relativistic correction $\kappa\Omega/2m$, by [see Eq. (47)]

$$V_{M,\gamma}(\mathbf{q}, \mathbf{k}) \approx \frac{ie}{2m} (\boldsymbol{\sigma}_1 - \boldsymbol{\sigma}_2) \cdot [\mathbf{k} \wedge \boldsymbol{\epsilon}^*(\lambda)]. \quad (52)$$

It shows no dependence on the nucleon momentum before emission \mathbf{q} . The Born amplitude associated to this approximation of the magnetic contribution reads then in spin space, using Eqs. (27) and (28) with $\mathbf{q}_2 = -\mathbf{q}$,

$$A_{p\bar{p}\gamma}^{M,(B,BC)}(\mathbf{q}, \mathbf{k}) = (2\pi)^3 \delta^{(3)}(\mathbf{q}_1 - \mathbf{q} + \mathbf{k}) V_{M,\gamma}(\mathbf{q}, \mathbf{k}) \tilde{G}_{p\bar{p}}(q). \quad (53)$$

We consider the $^3S_1 \rightarrow ^1S_0$ transition in the $p\bar{p}$ system. As read from Eq. (52) and discussed in Appendix C, the radiation from both baryons is described by $\boldsymbol{\sigma}_1 - \boldsymbol{\sigma}_2$. The related transition matrix element may be expressed in terms of the direction of spin in the triplet state, $\boldsymbol{\xi}$. Then, the relation

$$\langle 00 | \frac{1}{2} (\boldsymbol{\sigma}_1 - \boldsymbol{\sigma}_2) | 1 \boldsymbol{\xi} \rangle \cdot [\mathbf{k} \wedge \boldsymbol{\epsilon}^*(\lambda)] = \boldsymbol{\xi} \cdot [\mathbf{k} \wedge \boldsymbol{\epsilon}^*(\lambda)] \quad (54)$$

leads to a formula which may be used in the case of the limit defined by Eq. (52) for a transition from the $^3S_1 \rightarrow ^1S_0$ state. Indeed, from Eqs. (39), (47), and (53), we obtain

$$\begin{aligned} & \langle ^1S_0 | A_{p\bar{p}\gamma}^{M,(B,BC)}(\mathbf{q}, \mathbf{k}) | ^3S_1 \rangle \\ &= (2\pi)^3 \delta^{(3)}(\mathbf{q}_1 - \mathbf{q} + \mathbf{k}) \tilde{G}_{p\bar{p}}(q_r) \langle ^1S_0 | V_{M,\gamma} | ^3S_1 \rangle \\ &= (2\pi)^3 \delta^{(3)}(\mathbf{q}_1 - \mathbf{q} + \mathbf{k}) \tilde{A}_{p\bar{p}\gamma}^{M,(B,BC)}(\mathbf{q}, \mathbf{k}), \end{aligned} \quad (55)$$

with

$$\tilde{A}_{p\bar{p}\gamma}^{M,(B,BC)}(\mathbf{q}, \mathbf{k}) = \frac{ie}{m} \boldsymbol{\xi} \cdot [\mathbf{k} \wedge \boldsymbol{\epsilon}^*(\lambda)] \tilde{G}_{p\bar{p}}(q_r). \quad (56)$$

The electric contribution to the amplitude is

$$A_{p\bar{p}\gamma}^{E,(B,BC)}(\mathbf{q}, \mathbf{k}) = (2\pi)^3 \delta^{(3)}(\mathbf{q}_1 - \mathbf{q} + \mathbf{k}) V_{E,\gamma}(\mathbf{q}) \tilde{G}_{p\bar{p}}(q). \quad (57)$$

with the electric potential given in Eq. (40). In the same limit ($k/2m \ll 1$ and up to the relativistic correction $\kappa k^2/\Omega m$), the approximate electric potential reads

$$V_{E,\gamma}(\mathbf{q}, \mathbf{k}) \approx -\frac{e}{2m} 4 \mathbf{q} \cdot \boldsymbol{\epsilon}^*(\lambda). \quad (58)$$

It leads to transitions from the 1S_0 state to 3P states. However, final-state interactions in the P wave state are weak, at least in the Paris potential model, and they are therefore neglected.

On the other hand, in the magnetic transitions the scalar amplitude $A_{p\bar{p}\gamma}^{M,(0,BC)}(\mathbf{q}, \mathbf{k})$ has to be corrected and these corrections turn out to be very important. They are described by the loop integral [see Eq. (31)]

$$\begin{aligned} \tilde{A}_{p\bar{p}\gamma}^{M,(FSL,BC)}(\mathbf{q}_r, \mathbf{k}) &= \sum_{l=0,1} \int \frac{d\mathbf{q}'}{(2\pi)^3} T_l(\mathbf{q}_r, \mathbf{q}' - \mathbf{k}/2, E_{N\bar{N}}) \\ &\times G_{0,N\bar{N}\gamma}^+(\mathbf{q}', \mathbf{k}) \tilde{A}_{p\bar{p}\gamma}^{M,(B,BC)}(\mathbf{q}', \mathbf{k}), \end{aligned} \quad (59)$$

calculated with the recent Paris potential [8], in a way described in Ref. [15]. On shell, this T matrix element is normalized to the scattering length. The numerical evaluation of the loop integral in the presence of two singular propagators has to be done with considerable care. The procedure is described in Appendix E. The full amplitude for magnetic transitions becomes

$$\begin{aligned} A_{p\bar{p}\gamma}^{M,BC}(\mathbf{q}_1, \mathbf{q}_2, \mathbf{k}) &= (2\pi)^3 \delta^{(3)}(\mathbf{q}_1 + \mathbf{q}_2 + \mathbf{k}) \left[\tilde{A}_{p\bar{p}\gamma}^{M,(B,BC)}(\mathbf{q}_r, \mathbf{k}) \right. \\ &\left. + \tilde{A}_{p\bar{p}\gamma}^{M,(FSL,BC)}(\mathbf{q}_r, \mathbf{k}) \right], \end{aligned} \quad (60)$$

with \mathbf{q}_2 and \mathbf{q}_r given in Eq. (8).

For the results presented in the following section, the amplitude (60) has been evaluated with the potential $V_{M,\gamma}(\mathbf{q}, \mathbf{k})$ given in Eq. (41) including the $\kappa/2m$ relativistic correction but dropping the r_+ ($\sigma_1 + \sigma_2$) since this term generates spin triplet P waves only important close to the threshold region where they are strongly suppressed by the phase space.

V. THE RESULTS

A. The radiative decays

The $M(p\bar{p})$ data in the region of high photon energy are dominated by a peak, as can be seen in Figs. 5 and 6. The explanation is related to strong nucleon-antinucleon attraction essentially in $N\bar{N}$ the isospin-spin singlet 1S_0 state but to a certain extent also in the isotriplet spin singlet the 3S_0 . Now, with the radiation due to baryonic currents, this peak is strongly suppressed due to interference of the intermediate $p\bar{p}, n\bar{n}$ channels and the cancellations of the magnetic moments involved.

The various contributions to the $M_{p\bar{p}}$ spectrum plotted in Fig. 5 together with the experimental data have been obtained with the following procedure:

- $|F_0|$ is the overall normalization that is fixed by the $J/\psi \rightarrow p\bar{p}$ decay rate.
- Magnetic and electric amplitudes are calculated independently for the DE and BC emission modes.
- The emission rates are added and the normalizations of the DE and BC rates are fixed to reproduce the

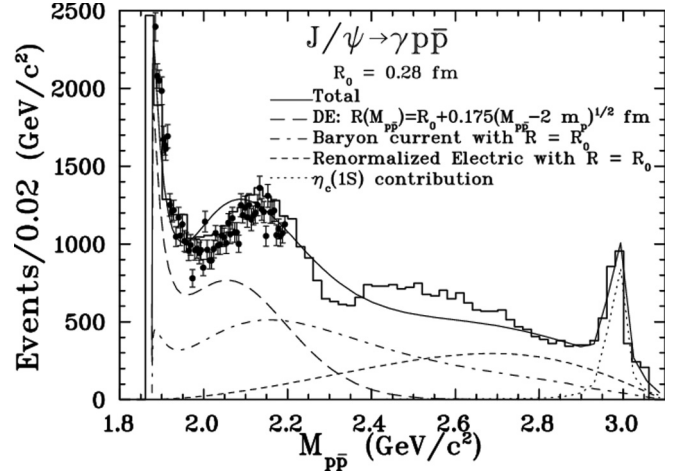


FIG. 5. The $M(p\bar{p})$ spectra obtained with the DE and baryon emission BC + FSI models. The peak at 3 GeV attributed to the sequential $J/\psi \rightarrow \eta_c \gamma$ decays is discussed in the text. Histogram as in Fig. 2; data extracted from Ref. [5].

experimental ratios shown in Table IV and the invariant mass distribution.

We are not able at present to evaluate the phase difference between the amplitudes associated to the DE and BC mechanisms. However, the interference effects are most likely fairly weak for two reasons:

- In the low- $M_{p\bar{p}}$ region, characterized by magnetic photons, the contribution of the DE mechanism dominates largely the contribution of the BC mechanism.
- In the high- $M_{p\bar{p}}$ region, a similar, although less striking, dominance is attributed to the electric photons, whereas there is practically no contribution any more of the DE mechanism.

The experimental data, displayed in Fig. 5, indicate possible interference effects in the region between 2.3 and 2.6 GeV. However, in view of the quality of the data, we hesitated to

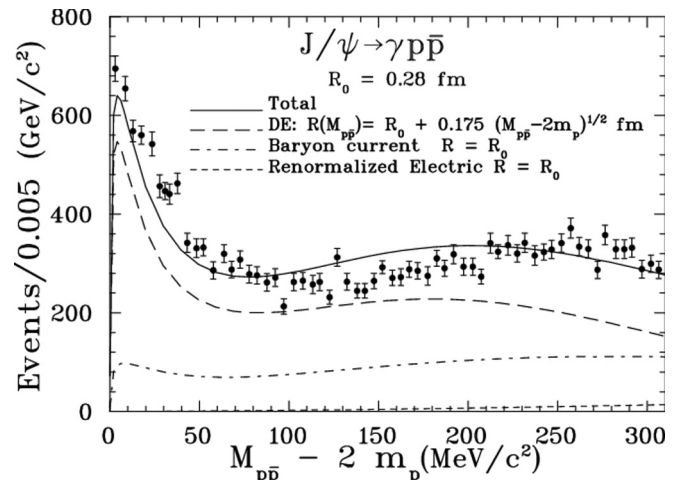


FIG. 6. As in Fig. 5 but for the near-threshold region. Note the small P -wave renormalized electric contribution.

TABLE IV. Ratio $\mathcal{R} = \Gamma(p\bar{p}\gamma)/\Gamma(p\bar{p})$ in % units with consecutive steps of improvement. The experimental ratio $\mathcal{R} = 18(5)$ is evaluated from the experimental branching fractions displayed in Table II. The first column indicates the involved mechanism: BC for the first line and BC + DE for the second. The other columns give the different contributions in these mechanisms (see text). The additional DE radiation arises from the quark phase and is fitted to the magnitude of the near-threshold peak.

Mechanism	Electric	Magnetic (BC)	Magnetic (BC + FSI)	Total
BC	4.38	1.65	1.97	6.35
BC + DE		5	6.51	12.86

include an additional parameter beyond the many parameters already introduced in our description. Thus, we have neglected the possible interferences and have simply added the contributions of the DE and BC mechanisms on the probability level.

The emission from final baryons (BC; see Table IV) generates about half of the experimental rate and misses the full strength of the threshold enhancement. Photons may be emitted also by exchange currents related to charged mesons exchanged between baryons. Such processes are known and well described in the NN systems, but to the best of our knowledge, have not been discussed in the $N\bar{N}$ systems. Calculations have been performed. We found effects of about 10% which do not change the overall picture in any significant way. The BC model has to be supplemented by the other internal emission DE mechanism discussed in Sec. III. The relative strength of the later is a free parameter which is set to try to reproduce the two peaks in $M(p\bar{p})$ spectrum (see Figs. 5 and 6). In this way, the total branching ratio becomes consistent with the data. The direct emission is characterized by different $N\bar{N}$ final-state interactions; in particular, there is no cancellation of p and n magnetic moments during the emission process. Hence, the interaction in the 1S_0 wave is stronger and the two resonances at threshold and at $M(p\bar{p}) \approx 2170$ MeV are more distinct. As discussed previously in Sec. III, the first is due to the quasibound state and the second is a shape resonance. Both are generated by the Paris potential model [8].

Now, a comparison of radiative decays $J/\psi \rightarrow \gamma p\bar{p}$ and $\psi(2S) \rightarrow \gamma p\bar{p}$ could be discussed qualitatively. The baryon current emission does not depend on the internal structure of the $J/\psi \rightarrow \gamma p\bar{p}$ and $\psi(2S) \rightarrow \gamma p\bar{p}$ mesons. What is shown in the present work is that the near-threshold peak is suppressed by the difference in the proton and neutron magnetic moments. On the other hand, the probability of internal photon radiation does depend on the internal structure. As a consequence, the relative weight of the two modes depends on the internal wave function, which is nodeless in the J/ψ case and has a node in the relative $c\bar{c}$ coordinate in the $\psi(2S)$ case. We are not able to calculate this wave function. Our qualitative argument is that the internal emission from the $\psi(2S)$ meson (that yields a peak) has to be small. Apparently, this node suppresses the magnetic radiative transitions via the DE mode and no peak is generated. We see some argument, although not fully convincing, for this suppression mechanism in the experimental $\gamma p\bar{p}$ branching ratios equal to $3.8(1.0) \times 10^{-4}$ for J/ψ and $3.9(0.5) \times 10^{-5}$ for $\psi(2S)$ (Ref. [21]).

a. *The end of $p\bar{p}$ spectrum.* The origin of the experimental peak at the end of spectrum is the sequential decay

$$J/\psi \rightarrow \eta_c \gamma \quad \text{and} \quad \eta_c \rightarrow p\bar{p}, \quad (61)$$

which generates a peak at the invariant mass $M(p\bar{p}) = M(\eta_c) = 2983.4$ MeV. The decay rates are known experimentally and $J/\psi \rightarrow \eta_c \gamma$ is $1.7 (0.4) \times 10^{-2}$ of the total while $\eta_c \rightarrow p\bar{p}$ is $1.50 (0.16) \times 10^{-3}$ of its decay rate [21]. The dotted line in Fig. 5 results from the modulus squared of the following relativistic Breit-Wigner amplitude for the description of the η_c ,

$$A_{\eta_c} = -f_{\eta_c} \frac{m_{\eta_c} \Gamma_{el}}{M_{p\bar{p}}^2 - m_{\eta_c}^2 + i m_{\eta_c} \Gamma_{tot}}, \quad (62)$$

with $\Gamma_{tot} = 31.8 (0.8)$ MeV and $\Gamma_{el}/\Gamma_{tot} = 1.50 (0.16) \times 10^{-3}$. In the energy range of this η_c contribution, the interference of the A_{η_c} amplitude with the very small magnetic S -wave is neglected and for the curve shown in Fig. 5 the free parameter f_{η_c} is fixed at the value 23.2×10^3 events / 0.02 (GeV/c²). Together, the expected area under the end peak would amount to 2×10^{-5} of the total decay rate, i.e., about 5% of the $p\bar{p}\gamma$ decay rate. The first experimental result of Ref. [4] indicated a 1% effect but more recent measurements yield comparable results [5].

In addition to the η_c peak, another peak arises within the BC model. It is related to the infrared enhancement in the intermediate-state $p\bar{p}$ propagator. The real infrared catastrophe does not occur since the initial J/ψ has a finite width. This effect produces an enhancement in the region $M(p\bar{p}) > 2820$ MeV and a narrow bump at the end $3090 < M(p\bar{p}) < 3100$ MeV. The area under this enhancement amounts to 3% of the rate \mathcal{R}_γ calculated with the baryon emission model. That is about 0.7% of the experimental rate. The experimental check is not easy as the errors in the photon energy determination (σ_E) are large in this region and these two effects overlap. The BES detector offers [4]

$$\frac{\sigma_E}{E} = \frac{21\%}{\sqrt{E/\text{GeV}}}, \quad (63)$$

and in the region of interest $\sigma_E \approx E \approx 100$ MeV and thus the position of the peak is not well determined. With a better resolution, the magnitude and shape of the infrared bump would be a check for decay models.

As indicated in Sec. IV A, in the comment below Eq. (34), the BES data [5], where a $k < 50$ MeV/c cut is applied, does not display the contribution of the infrared photon contribution. Thus, in the present work, the $M_{p\bar{p}}$ infrared pole is eliminated by introducing a smooth nonrelativistic Breit-Wigner function. In other terms, a phenomenological final-state interaction correction is applied to the P -wave electric amplitude $A_{p\bar{p}\gamma}^{E,(B,BC)}(\mathbf{q}, \mathbf{k})$ given by Eq. (57). Hence, the short-dashed line in Fig. 5 is the result of the renormalized electric photon amplitude where the $M_{p\bar{p}} = M_{J/\psi}$ pole has been eliminated:

$$\begin{aligned} \tilde{A}_{p\bar{p}\gamma}^{E,(B,BC)}(\mathbf{q}, \mathbf{k}) &= f_r A_{p\bar{p}\gamma}^{E,(B,BC)}(\mathbf{q}, \mathbf{k}), \quad (64) \\ f_r &= \left| N_E \frac{M_{J/\psi} - M_{p\bar{p}}}{M_{J/\psi} - M_{p\bar{p}} - i\Gamma_E} \right|. \quad (65) \end{aligned}$$

TABLE V. Calculated ratios $\Gamma(p\bar{p} \text{ meson})/\Gamma(p\bar{p})$ of channel widths allowed in the J/ψ decays. The errors correspond to uncertainties of the $p\bar{p}$ meson coupling g . Values of \mathcal{R}_{exp} calculated from the experimental branching fractions listed in Table II.

Meson	\mathcal{R}_{exp}	$\mathcal{R}[\text{BC}]$	$\mathcal{R}[\text{BC,FSI}]$	$\mathcal{R}[\text{BC,FSI,DE}]$	$g^2/(4\pi)$
$p\bar{p}\pi^0$	0.575 (0.05)	0.43			13.8 [27]
$p\bar{p}\pi^-$	0.966 (0.06)	0.85			13.8 [27]
$p\bar{p}\omega$	0.507 (0.07)	0.87 (0.16)	0.67 (0.13)		8.1 (1.5) [26]
$p\bar{p}\phi$	0.507 (0.07)	0.40	0.33	0.39	4.16 [29]
$p\bar{p}\phi$	0.0247 (0.0016)	0.023			5.5 this work

The free parameters are fixed at the respective values $\Gamma_E = 500$ MeV for the width and $N_E = 3.5$ for the normalization.

Despite the Breit-Wigner form, we do not suggest that there is a new resonant mechanism involved. This form is used only for a parametrization that serves two purposes:

- (1) removing the infrared enhancement since it is removed in the experimental data and
- (2) enhancing the electric photon emission approximately by a factor 3 to reach consistency with the data.

Although a new resonance is a possibility, we are inclined to view f_r in Eq. (65) as a result of another DE mechanism. This possibility is discussed in the next subsection devoted to the ω emission and where, indeed, the broad bump in the spectrum is due to the DE decay mode and not to an intermediate resonance. A quantitative analysis may be performed in the ω emission case as more data exist. It is not feasible in the radiative decay mode and we limit the analysis to the phenomenological formula (64).

B. The ω, ϕ , and π emission rates

1. The ω emission

Its rate seems to be easier to understand than those for the radiative decays due to the weak tensorial coupling, which favors strongly the electric-type transitions. The corresponding

branching fraction

$$\mathcal{R}_\omega = \frac{\Gamma(p\bar{p}\omega)}{\Gamma(p\bar{p})} \quad (66)$$

obtained with the basic final-state emission (BC) model is shown in Table V. The electric-type transitions (E) lead to P -wave $p\bar{p}$ states with small final-state interactions. The magnetic-type transitions (M) generate S wave states strongly affected by the final $N\bar{N}$ interactions. In comparison to the photon case, these interactions are stronger as isospin conservation requires baryons to be in isospin-0 state. On the other hand, due to large meson mass, the final p and \bar{p} are less strongly oriented close to threshold and the tensor $NN\omega$ coupling is weak and consistent with zero. Hence, effects of these final-state interactions are not very visible in the emission rate; see Fig. 7. It is the electric transition (labeled EE in Fig. 7) that dominates. Now, in distinction to the photon case, the longitudinal component $\epsilon^*(\lambda=0)$ exists and the corresponding strength of the dominant electric transition is given in Eq. (D30). It yields approximately $(g_{V\omega q}/2m)^2$. One finds that the longitudinal component gives a large contribution to the low part of the $M_{p\bar{p}}$ spectrum, which is not supported by the data.

The decay rates are given in Table V and these results are obtained with the coupling constant $g_V^2(NN\omega)/4\pi = 8.1$ (1.5), $g_T^2(NN\omega)/4\pi = 0.16$ (0.46) obtained with

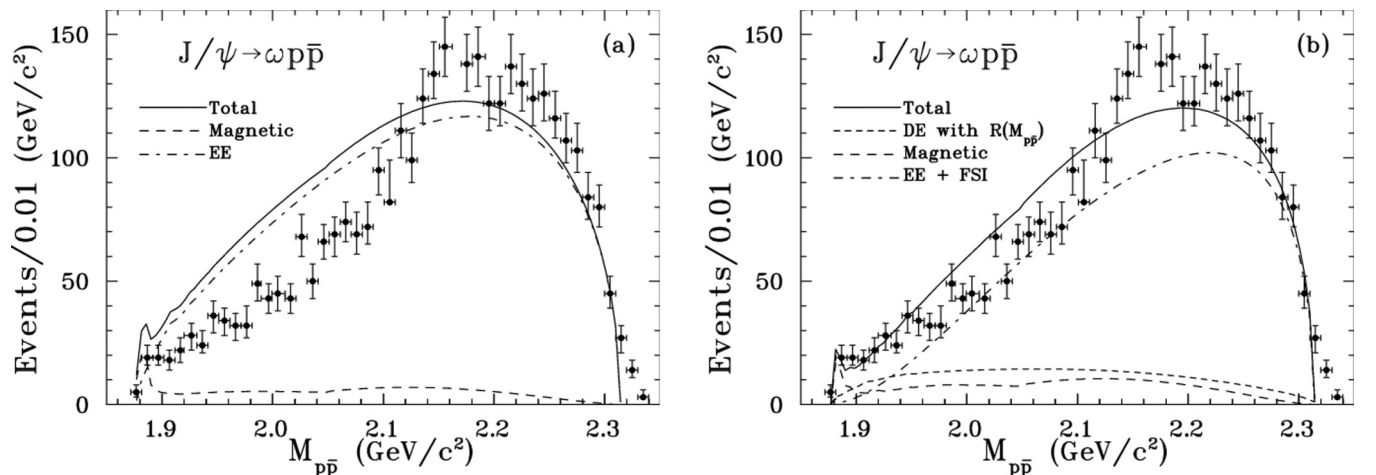


FIG. 7. Left panel (a): the $M_{p\bar{p}}$ spectrum obtained with the BC model. Right panel (b): the $M_{p\bar{p}}$ spectrum obtained with the BC + FSI model. The same arbitrary normalization is used to fit the experimental shape for both graphs. The electric contribution is labeled EE. No FSI contribution in the DE model but the weak energy dependence of the source radius [Eq. (24)] has been kept. Here $R_0 = 0.28$ fm, $g_{V\omega}^2/(4\pi) = 3.8$, and $g_{T\omega} = 0$. Data extracted from Fig. 2 in Ref. [18].

dispersion relations [26]; more recent values from NN interactions are $g_V^2(NN\omega)/4\pi = 9.73$, $g_T^2(NN\omega)/4\pi = 0.005$ [27]. In both cases, the tensorial coupling is negligible and it was neglected. However, the most significant parameter is the source radius and the rates of ω (and π) meson emissions put very strong limits on R_0 . The final choice is obtained from the best fit of \mathcal{R}_ω and \mathcal{R}_π is $R_0 = 0.28(1)$. The ω coupling constants are uncertain; those indicated above are extracted from NN scattering data. On the other hand, coupling constants derived from semiphenomenological meson formation data are smaller. A value $g_V^2(NN\omega)/4\pi = 1.19$ has been obtained in Ref. [28] with a very small tensorial coupling, although Ref. [29] reaches a value $g_V^2(NN\omega)/4\pi = 4.16$. In our calculations, we have chosen $g_V^2(NN\omega)/4\pi = 3.8$ and $g_T(NN\omega) = 0$.

The ω emission case differs strongly from the photon emission as apparently the BC mode dominates. However, as already shown in the BES Collaboration paper [18], the emission of ω mesons requires the involvement of excited nucleon states N^* and the final state involves three interacting particles. The multiple scattering method presented here requires the leading corrections due to N^* to reach some 25% of the leading order. Roughly the next (missing) order is expected to reach about 10%. Such corrections are unlikely to be kept under control as the quantum numbers of N^* resonances are very uncertain. Thus one will have to resort to more appropriate methods than that of the simple DWBA used in the present work to achieve more reliable results. Also, one has to keep in mind that the basic term involves a rather uncertain $NN\omega$ coupling constant, which makes the calculations even less (if not) reliable if this coupling turns out to be much smaller.

2. The $M_{p\bar{p}}$ and $M_{\omega p}$ spectra

The BC model of meson emission from final baryons yields a fair estimate of the decay rate, Table V, unfortunately subject to large uncertainty in the ωNN coupling constant. On the other hand, the spectra of the invariant masses $M_{p\bar{p}}$ and $M_{\omega p}$ pose a more difficult problem. The $M_{p\bar{p}}$ distribution, plotted in the left panel of Fig. 7, requires strong reduction in the lower mass region, which may be generated only by a destructive interference. Such a possibility is offered by final-state interactions involving a $N(3/2^-)$ resonant state expected to mediate the ω - p interaction in the 2-GeV energy region [see Fig. 9(b)]. Now, the bulk of available phase space covers region between $M_{\omega p} = 2052$ MeV at $p\bar{p}$ threshold and $M_{\omega p} = 1805$ MeV at the end of $M_{p\bar{p}}$ spectrum. Hence, interference of the intermediate $N(3/2^-)$ and the basic decay mode may be constructive in part and destructive in another part of the phase space.

The related mechanism is presented only schematically here. The Rarita-Schwinger particle propagation is given by

$$G^{\mu\nu} = \frac{\gamma p + m_{3/2}}{m_{3/2}^2 - p^2 + im_{3/2}\Gamma} P^{\mu\nu}, \quad (67)$$

where $P^{\mu\nu}$ projects on spin-3/2 states. We follow Ref. [30], which underlines some controversies in the formulation. These are of small concern as in the situation discussed here one finds

this particle to be nonrelativistic and [31]

$$P^{\mu\nu} \rightarrow P^{ij} = 2/3[\delta^{ij} + i/2\epsilon_{ijk}\sigma^k]. \quad (68)$$

This formula sets the main simplification of this final-state interaction. In addition, we drop the second term, which leads to spin flip, leading to no interference with the basic Born amplitude. The calculation involves a standard loop integral which follows the procedure of Appendix E. Three uncertain parameters are implied: We use $m_{3/2} = 2050$ MeV, $\Gamma = 300$ MeV for the $N(3/2^-)$ position and width (nonessential), and 3% for the strength of the $N(3/2^-)$ coupling to the $\omega - N$ channel. The effect is shown in Figs. 7(b) and 10. The resonance parameters ($m_{3/2} = 2050$ MeV, $\Gamma = 300$ MeV) are close to those of the $N(1875)$ and of the more uncertain $N(2120)3/2^-$ resonances (see Ref. [21]).

On the other hand, the ω spectra are not reproduced and the $M_{\omega p}$ and $M_{\omega\bar{p}}$ distributions miss a bump in the data at large masses. Inspection of Fig. 10 indicates a broad structure missing around 2 GeV. Such resonance has been already introduced into our description of the final-state interaction. Nevertheless, its effect is not seen in the distribution of $M_{\omega\bar{p}}$ [18]. The formalism developed so far indicates a strong correlation of $M_{\omega p}$ and $M_{p\bar{p}}$. The phase space region close to the $p\bar{p}$ threshold overlaps with the region of $M_{\omega p} \sim 2.05$ GeV. Thus, enhancing the high-energy tail of $M_{\omega p}$ reduces the low-energy end of $M_{p\bar{p}}$. Within the BC + FSI approach, it is not possible to reproduce both distributions and another mechanism has to be found. Another option tried was $J/\psi \rightarrow \bar{N}(1/2^-)N^*(3/2^-) \rightarrow \bar{N}N\omega$, but for the reason given above it was not able to explain simultaneously the $M_{p\bar{p}}$ and the $M_{\omega p}$ spectra.

As the introduction of resonances brings no success, we resort to another formation mechanism which was found useful in the study of radiative decays. A fraction of ω mesons is assumed to be emitted internally i.e., before the baryons are formed in a P wave state. This emission process is depicted in Fig. 1(a), where the photon line is replaced by an ω -meson line. Instead of the matrix element given by Eq. (14) related to S states, that associated to P states should be of the form

$$V_\omega^{\text{DE}}(\lambda) = f \epsilon^*(\lambda) \cdot \xi, \quad (69)$$

where f is a free coupling constant. In the center-of-mass (c.m.) system of J/ψ , the bilinear form of V_ω^{DE} averaged over directions of ξ leads to sum over polarizations

$$\sum_{\lambda=-1}^1 |(V_\omega^{\text{DE}}(\lambda))|^2 = f^2 \sum_{\lambda} \epsilon_i^* \epsilon^i = f^2 (3 - \mathbf{k}^2/m_\omega^2). \quad (70)$$

Now the essential point is that this coupling does not depend on q^2 in contrast to the helicity sum of $|V_E^\omega|^2(\lambda)$ in Eq. (D30). Jointly with the assumed expansion of the system during the decay expressed in Eq. (24), one is able to avoid the unrequired correlation of low-energy $M_{p\bar{p}}$ and high-energy $M_{\omega p}$. Here, final-state interactions are not introduced in the direct emission (DE) model but the same weak energy dependance for the source radius [Eq. (24)] as for the photon case has been kept, i.e., $R_0 = 0.28$ fm and $\beta = 0.175$ fm^{3/2}. The strength of coupling to V_ω^{DE} is obtained by the best fit to both $M_{p\bar{p}}$ and $M_{\omega p}$ spectra. The results are given in Figs. 7 and 10. It is apparent

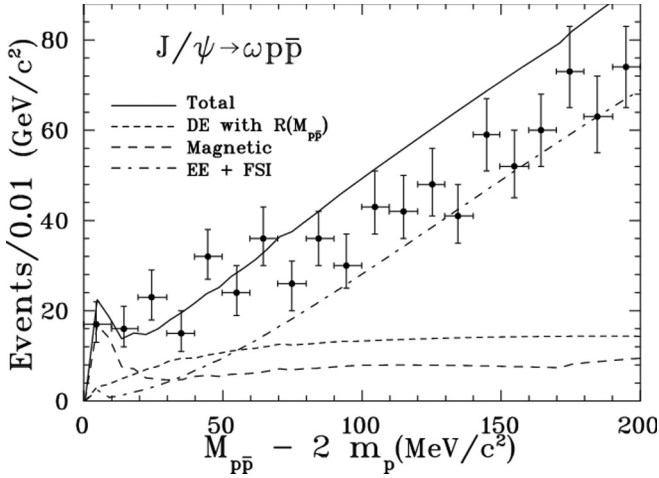


FIG. 8. The $M_{p\bar{p}}$ spectrum as in Fig. 7(b) but for the near-threshold region.

that the bump in the last figure is not due to a resonance but to a different decay mode. This internal emission mode contributes about 22% of the decay rate.

3. The π and ϕ emission rates

They are given in Table V. The neutral pion is emitted coherently from the intermediate $p\bar{p}$ system. The negatively charged pion may be emitted from the antiproton only. However, in the intermediate $I = 0$ state, one has also $n\bar{n}$ component and the π^- may be emitted by the neutron. These processes are coherent. Therefore, the ratio $\Gamma(p\bar{n}\pi^-)/\Gamma(p\bar{p}\pi^0) = 1.78(0.22)$ within error limits equals 2 minus the square of the relevant pion-nucleon coupling constants. This indicates that pions are emitted predominantly in the baryonic phase of decay and that final-state interactions are not essential, the $p\bar{p}$ and $p\bar{n}$ interactions being different. The BES data indicate effects of N^* resonances in the invariant mass distribution which, depending on the way of description, amount to some 25% of the total rate.

The ϕ experimental branching ratio is small as the allowed phase space is small. Table V shows that it may be obtained with the value $g_V^2/4\pi = 5.5, g_T = 0$, which compares well with $g_V^2/4\pi = 5.1, g_T^2/4\pi = 0.2$ obtained in Ref. [32]. The experimental spectra obtained by the BES III Collaboration [22] for the $J/\psi \rightarrow p\bar{p}\phi$ are qualitatively very close to those obtained in the $J/\psi \rightarrow p\bar{p}\omega$ case (see Figs. 8 and 10). So the

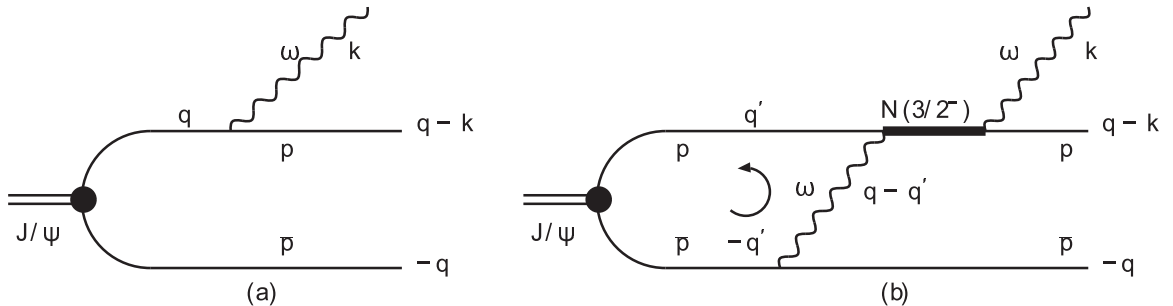


FIG. 9. Emission of the ω meson from intermediate baryons. The left graph (a) corresponds to the Born term while the right one (b) includes final-state corrections involving the $N(3/2^-)$ nucleon resonance.

basic BC mode is likely to require corrections on the same 25% level as in the ω case, notwithstanding that the missing knowledge of the ϕ coupling to N^* or Δ^* resonances and uncertainties in the ϕNN coupling constants do not allow a more precise discussion. The present accurate experimental value [22] for the ratio $\mathcal{R}(p\bar{p}\phi)/\mathcal{R}(p\bar{p})$ favors clearly the necessity of a more elaborate approach than just relying on the Born term of the baryon current considered in this study. But this would be the subject of a research project by itself.

VI. SUMMARY AND OUTLOOK

A. Summary

In the present work, the $J/\psi \rightarrow \mathcal{B}p\bar{p}$ decays where $\mathcal{B} = \gamma, \omega, \phi, \pi$ have been studied. Two processes have been introduced to describe the BES Collaboration data on the photon [4,5] or ω meson [17,18] formation in J/ψ decays into $p\bar{p}$. For the radiative decays, both processes include final-state nucleon-antinucleon interactions with S -wave half-off shell functions [15] based on the Paris NN potential [8]. The J/ψ source is described in momentum space by a phenomenological Gaussian function with radius R_0 [see Eq. (9)]. The value $R_0 = 0.28$ fm is found to be the best choice to reproduce the different particle \mathcal{B} decay rates as compared to that of the $J/\psi \rightarrow p\bar{p}$ decay. Before presenting some outlook, the description of the two mechanisms and of the free parameters for the photon and meson emissions are summarized below.

- (1) *Direct emission process.* Here, the emission of photons or ω mesons occurs before the final baryons are formed. In the radiative decay, the final-state interactions generate two distinct final resonant states in the $p\bar{p}$ system. One close to the threshold (very sharp peak in the $p\bar{p}$ spectra) is explained as an effect of baryonium—a broad 52-MeV-wide quasibound state at 4.8 MeV below threshold generated in the $^{11}S_0$ wave by the Paris potential. Another—a resonant state at 2170 MeV—is formed as a shape resonance in the same partial wave. The Born contribution of the direct emission process allows to achieve a good description of the full ω spectrum at large $M_{p\bar{p}}$ and $M_{\omega p}$ invariant masses. For the γ or ω meson, it is found necessary to introduce, for the source radius, a weak energy dependence on $M_{p\bar{p}}$ [see Eq. (24)], and in both cases the same dependence is used.

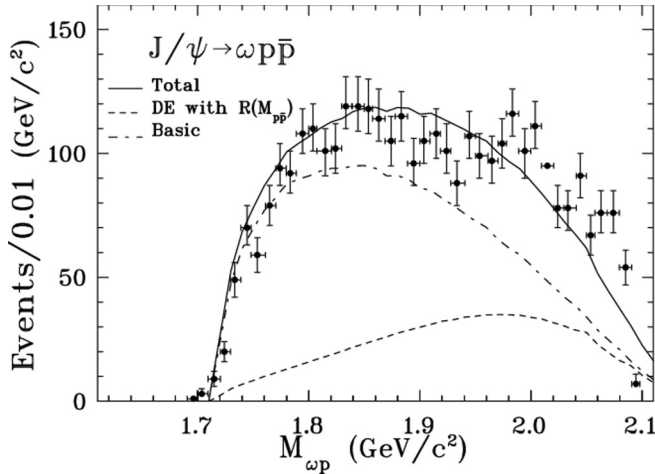


FIG. 10. The $M_{\omega p}$ spectrum obtained with the BC + FSI + DE model (see Fig. 7 caption). The dash-dotted curve (Basic model) refers to the BC + FSI calculation.

- (2) *Emission from baryonic current.* The second mechanism assumes the emission of photons (or mesons) by the baryonic currents in the final state of the $J/\psi \rightarrow p\bar{p}$ decay. This emission occurs thus after the initial decay of the J/ψ into an $N\bar{N}$ pair. In the radiative decay channel, this process is not sufficient to provide a fair reproduction of final resonant states. This is the reason why this model has to be completed by the direct emission model just described above. For the ω -meson production case, the Born term of this process is the dominant mode as it is in the π or ϕ formation case. However, the ω invariant mass distribution $M_{p\bar{p}}$ requires a strong reduction in the lower mass region. This is obtained by introducing a specific final-state interaction involving a $N^*(3/2)$ or $\bar{N}^*(3/2)$ resonance created by an ω - p (ω - \bar{p}) interaction through an ω -meson exchange between the $\bar{p}(p)$ and $p(\bar{p})$ pairs [see Fig. 9(b)].
- (3) *Free parameters for the radiative emission.* For the photon emission case, to reproduce the $M_{p\bar{p}}$ spectra (see Figs. 5 and 6) and the relative decay rate (see Table IV), *seven free parameters* are used: The initial radius of the source function, $R_0 = 0.28$ fm, the slope parameter associated to the energy dependence of this radius $\beta = 0.175$ fm^{3/2}, the normalization of the direct emission model contribution [Eq. (22)], that of the baryon current contribution [Eq. (33)], the coefficients $\Gamma_E = 500$ MeV and $N_E = 3.5$ entering the renormalized electric photon amplitude [Eq. (64)] and the normalization f_{η_c} for the η_c Breit-Wigner parametrization in Eq. (62).
- (4) *Free parameters for the meson emissions.* In the case of the ω -meson emission, to fit the invariant masses $M_{p\bar{p}}$ and $M_{\omega p}$ distributions (see Figs. 7 and 10) and the relative decay rate (see Table V), *five free parameters* are introduced: the normalization of the BC + FSI

model [see Eqs. (33), (48), (D30), and (D33)], the two $N(3/2^-)$ parameters in Eq. (67), viz., $m_{3/2} = 2050$ MeV, $\Gamma = 300$ MeV plus the 0.3% strength of its coupling to $N\omega$ and the direct ω -emission coupling constant f [see Eq. (70)]. Looking at the ratio of the decay rates $\mathcal{R}(p\bar{p}\omega)/\mathcal{R}(p\bar{p})$ given in Table V, a $g_{V\omega}^2/4\pi$ coupling between 4.16 and 8.1 would bring this ratio closer to the experimental value. This table also shows that the Born amplitude [Eq. (27)] allows us to reproduce well the relative decay rates for the cases of the π or ϕ emission for known values of $g^2(p\bar{p}\pi)$ or $g^2(p\bar{p}\phi)$.

- (5) *Uncertainties, shortcomings.* The basic mechanism for pion emission from the baryonic currents yields decay rates smaller than the experimental ones (see Table V). A proper description of the proton-pion invariant mass distribution requires at least three pion-nucleon resonant states and a good control over relative phases [34]. The limitation to single dominant final partial wave is not sufficient to describe the rather precise data. For radiative decays, the separation of two formation mechanisms is only approximate due to two effects:
 - (a) unknown relative phase of both amplitudes may affect the region $M_{p\bar{p}} \approx 2.45 \pm 0.15$ GeV where these mechanisms give comparable rates, and
 - (b) there might be some presumably weak effect of the isospin symmetry violation in the course of the internal photon emission.

Both effects are difficult to calculate.

B. Outlook

Because the internal structures of the J/ψ and $\psi(2S)$ are different, the direct emission model is less likely to give a reasonable description of the radiative decay of the $\psi(2S)$ state. This might explain, in a qualitative way, why no resonant states are visible in this process.

The phenomenological part of the $N\bar{N}$ Paris potential [8] has been determined to reproduce the $N\bar{N}$ data up to $E_{N\bar{N}} \approx 200$ MeV, i.e., $M_{p\bar{p}} \approx 2.1$ GeV. It is interesting to observe that nevertheless it produces reasonable results beyond the region tested in scattering experiments. The present approach could also be applied with other $N\bar{N}$ scattering matrices, for instance, that of Ref. [33]. Furthermore, with more accurate experimental results, effects of weakly populated final $N\bar{N}$ states might enter. In the present study, they do not seem to give sizable contributions.

Complications were found for the ω emission channel: The $M_{p\bar{p}}$, $M_{\omega p}$ and $M_{\omega\bar{p}}$ spectra [18] might indicate contributions of two N^* states. The description of these is complementary to that of the mesic and radiative excitations of the nucleon. With increased precision of the BES Collaboration measurements, the extraction of the resonance parameters and nucleon-meson coupling constants should be more accurate.

Spectra of the $J/\psi \rightarrow p\bar{p}\pi^0$ decays (see, e.g., Ref. [34]), although not discussed here, indicate at least effects of established $N(1535)$ and $N(1650)$ states. The description of

these decays seems to be a pressing question which may yield more information than those arising from the uncertain ω case.

The infrared catastrophe is approached by the baryon current model. It would thus be interesting to improve the energy resolution at the end of the spectrum to validate or disprove the photon (light meson) emission process from the final baryons.

Finally, the present work should allow us to approach the related $\bar{p}p \rightarrow J/\psi + \text{meson}$ reaction on nuclei, which sooner or later will be studied experimentally [1].

ACKNOWLEDGMENT

Support from the French-Polish COPIN/IN2P3-PAN Collaboration Agreement No. 05-115 is gratefully acknowledged.

APPENDIX A: PHASE SPACE

Let $p = (p_0, \mathbf{p})$,

$$p^2 = p_0^2 - \mathbf{p}^2, \quad \text{and} \quad p_0 = E(\mathbf{p}) = E(|\mathbf{p}|) = E(p) = \sqrt{\mathbf{p}^2 + m^2}.$$

Then the restricted two-body phase space for the $J/\psi \rightarrow p\bar{p}$ decay at rest reads, with q_1 and q_2 denoting the four-momenta of the nucleon and the antinucleon with masses $m_1 = m_2 = m$,

$$\begin{aligned} L_2 &= (2\pi)^4 \int \prod_{i=1,2} \frac{d^4 q_i}{(2\pi)^3} \theta(q_i^0) \delta(q_i^2 - m_i^2) \delta^{(3)}(\mathbf{q}_1 + \mathbf{q}_2) \delta(M_{J/\psi} - E(\mathbf{q}_1) - E(\mathbf{q}_2)) \\ &= \frac{1}{4\pi} \int \frac{q^2 dq}{E^2(q)} \delta(M_{J/\psi} - 2E(q)) = \frac{1}{8\pi} \frac{\sqrt{M_{J/\psi}^2 - 4m^2}}{M_{J/\psi}}, \end{aligned} \quad (\text{A1})$$

which is numerically equal to 0.03164.

For a J/ψ at rest decaying into a $p\bar{p}\mathcal{B}$ channel with respective four-momenta q_1, q_2 , and k , the three-body phase space reads

$$\begin{aligned} L_3 &= (2\pi)^4 \int \prod_{i=1,2} \frac{d^4 q_i}{(2\pi)^3} \theta(q_i^0) \delta(q_i^2 - m_i^2) \frac{d^4 k}{(2\pi)^3} \theta(k_i^0) \delta(k^2 - m_{\mathcal{B}}^2) \delta^{(3)}(\mathbf{q}_1 + \mathbf{q}_2 + \mathbf{k}) \delta(M_{J/\psi} - E(\mathbf{q}_1) - E(\mathbf{q}_2) - E_{\mathcal{B}}(\mathbf{k})) \\ &= \frac{1}{(2\pi)^5} \int \frac{d\mathbf{q}_1}{2E(\mathbf{q}_1)} \int \frac{d\mathbf{q}_2}{2E(\mathbf{q}_2)} \int \frac{d\mathbf{k}}{2E_{\mathcal{B}}(\mathbf{k})} \delta(\mathbf{q}_1 + \mathbf{q}_2 + \mathbf{k}) \delta(M_{J/\psi} - E(\mathbf{q}_1) - E(\mathbf{q}_2) - E_{\mathcal{B}}(\mathbf{k})) \\ &= \frac{1}{(2\pi)^5} \int \frac{d\mathbf{q}}{2E(\mathbf{q})} \int \frac{d\mathbf{k}}{2E_{\mathcal{B}}(\mathbf{k}) 2E(-\mathbf{q} - \mathbf{k})} \delta(f(x)) \end{aligned} \quad (\text{A2})$$

with

$$x = \frac{\mathbf{k} \cdot \mathbf{q}}{k q} \quad (\text{A3})$$

and

$$f(x) = M_{J/\psi} - E(q) - \sqrt{k^2 + q^2 + 2kq x + m^2} - E_{\mathcal{B}}(k). \quad (\text{A4})$$

Thus, energy conservation implies that $f(x)$ cancels for

$$x = x_0 = \frac{M_{p\bar{p}}^2 - 2E(q)[M_{J/\psi} - E_{\mathcal{B}}(k)]}{2kq} \quad (\text{A5})$$

and we have introduced the invariant nucleon-antinucleon invariant mass squared

$$M_{p\bar{p}}^2 = s = [M_{J/\psi} - E_{\mathcal{B}}(k)]^2 - k^2. \quad (\text{A6})$$

The invariant $N\bar{N}$ mass spans the interval $[2m, M_{J/\psi} - m_{\mathcal{B}}]$. Then, we have

$$L_3 = \frac{1}{(2\pi)^3} \int_0^\infty \frac{k^2 dk}{2E_{\mathcal{B}}(k)} \int_0^\infty \frac{q^2 dq}{2E(q)} \int_{-1}^1 dx \frac{\delta(f(x))}{\sqrt{k^2 + q^2 + 2kq x + m^2}} = \frac{1}{(2\pi)^3} \int_0^\infty \frac{k dk}{2E_{\mathcal{B}}(k)} \int_0^\infty \frac{q dq}{2E(q)} \int_{-1}^1 dx \delta(x - x_0). \quad (\text{A7})$$

From Eq. (A5), where one has $-1 \leq x_0 \leq 1$, one gets $1 - x_0^2 \geq 0$ so that

$$4k^2 q^2 (1 - x_0^2) = -4M_{p\bar{p}}^2 E^2(q) + 4[M_{J/\psi} - E_{\mathcal{B}}(k)] E(q) M_{p\bar{p}}^2 - (M_{p\bar{p}}^4 + 4m^2 k^2)$$

must be positive. Hence, $E(q)$ will lie between the two positive roots, E_+ and E_- , of the trinomial

$$E_{\pm} = \frac{(M_{J/\psi} - E_B(k))}{2} \pm \frac{k}{2 M_{p\bar{p}}} \sqrt{M_{p\bar{p}}^2 - 4m^2}, \quad (\text{A8})$$

where $E_- > m$ and, from Eq. (A6), k is a function of the invariant mass $M_{p\bar{p}}$

$$k = k(M_{p\bar{p}}) = \frac{\sqrt{[(M_{J/\psi} + m_B)^2 - M_{p\bar{p}}^2]} [(M_{J/\psi} - m_B)^2 - M_{p\bar{p}}^2]}{2M_{J/\psi}} = \frac{\sqrt{\lambda(m_B^2, M_{J/\psi}^2, M_{p\bar{p}}^2)}}{2M_{J/\psi}}, \quad (\text{A9})$$

where we have introduced the standard triangle (Källén) function $\lambda(x, y, z)$.⁴

We may now transform the remaining integrations using $q \, dq/E(q) = dE$ and from Eq. (A6) changing the variable k to $M_{p\bar{p}}$ to obtain

$$L_3 = \frac{1}{(2\pi)^3} \int_{2m}^{M_{J/\psi} - m_B} \frac{M_{p\bar{p}} \, dM_{p\bar{p}}}{4M_{J/\psi}} (E_+ - E_-) = \frac{1}{(2\pi)^3} \frac{1}{4M_{J/\psi}} \int_{2m}^{M_{J/\psi} - m_B} k(M_{p\bar{p}}) \sqrt{M_{p\bar{p}}^2 - 4m^2} \, dM_{p\bar{p}} \quad (\text{A10})$$

and arrive at

$$\begin{aligned} L_3 &= \frac{1}{(2\pi)^3} \frac{1}{8 M_{J/\psi}^2} \int_{2m}^{M_{J/\psi} - m_B} \sqrt{\lambda(m_B^2, M_{J/\psi}^2, M_{p\bar{p}}^2)} [M_{p\bar{p}}^2 - 4m^2] \, dM_{p\bar{p}} \\ &= \frac{1}{(2\pi)^3} \frac{1}{16 M_{J/\psi}^2} \int_{4m^2}^{(M_{J/\psi} - m_B)^2} \frac{du}{u} \sqrt{\lambda(m_B^2, M_{J/\psi}^2, u) \lambda(m^2, m^2, u)}. \end{aligned} \quad (\text{A11})$$

In the case where the vector particle is a photon, the integral (A11) can be calculated exactly (see, e.g., Ref. [35]) and gives

$$L_{3,\gamma} = \frac{1}{32\pi^3} \left\{ \frac{M_{J/\psi}^2 + 2m^2}{8 M_{J/\psi}} \sqrt{M_{J/\psi}^2 - 4m^2} - \frac{m^2 (M_{J/\psi}^2 - m^2)}{M_{J/\psi}^2} \ln \left[\frac{M_{J/\psi} + \sqrt{M_{J/\psi}^2 - 4m^2}}{2m} \right] \right\}, \quad (\text{A12})$$

which is numerically equal to 261.718 (MeV)².

APPENDIX B: THE WIDTH FOR $J/\psi \rightarrow p \bar{p} B$ DECAY PROCESS

Let us evaluate the decay amplitude in the Born approximation, the boson being radiated either from the proton or from the antiproton. If we let the proton radiate, the left panel on Fig. 4 indicates that $\mathbf{q}_1 = \mathbf{q} - \mathbf{k}$ denotes the momentum of the proton after the photon emission while $\mathbf{q}_2 = -\mathbf{q}$ is the spectator antiproton final momentum and \mathbf{k} is the boson momentum. Then, the potential $U_{p\bar{p}B}^0(\mathbf{q}_1, \mathbf{k})$ can be expressed as [Eq. (38)]

$$U_{p\bar{p}B}^0(\mathbf{q}_1, \mathbf{k}) = A_{V,B}(\mathbf{q}_1, \mathbf{k}) + \frac{i\kappa}{2m} A_{T,B}(\mathbf{q}_1, \mathbf{k}) \quad (\text{B1})$$

with κ being the anomalous magnetic moment. From this expression, one then evaluates the associated amplitude [Eq. (28)] $A_{p\bar{p}B}^{B,BC}(\mathbf{q}_1, \mathbf{k})$ which is still an operator in the spin-isospin space. From Eqs. (27) and (28), we obtain the probability for the decay with a boson emission

$$\Gamma(p\bar{p}B) = \frac{1}{(2\pi)^5} \int \frac{d\mathbf{q}_1 \, d\mathbf{q}_2 \, d\mathbf{k}}{2E(q_1)2E(q_2)2E_B(k)} \delta(M_{J/\psi} - E(q_1) - E(q_2) - k) \delta^{(3)}(\mathbf{q}_1 + \mathbf{q}_2 + \mathbf{k}) |A_{p\bar{p}B}^{B,BC}(\mathbf{q}_2, \mathbf{k})|^2. \quad (\text{B2})$$

For a boson emission of mass m_B with an energy $E_B(k) = \sqrt{m_B^2 + k^2}$, we have

$$\begin{aligned} \Gamma(p\bar{p}B) &= \frac{1}{(2\pi)^5} \int \frac{d\mathbf{q} \, d\mathbf{k}}{2E(q) \, 2E(|\mathbf{q} + \mathbf{k}|) \, 2E_B(k)} \delta(M_{J/\psi} - E(q) - E(|\mathbf{q} + \mathbf{k}|) - E_B(k)) |A_{p\bar{p}B}^{B,BC}(\mathbf{q}, \mathbf{k})|^2 \\ &= \frac{1}{(2\pi)^4} \int \frac{d\mathbf{q}}{2E(q)} \int \frac{k^2 dk}{2E_B(k)} \int dx \frac{\delta(f(x))}{2E(|\mathbf{q} + \mathbf{k}|)} |A_{p\bar{p}B}^{B,BC}(\mathbf{q}, k, x)|^2, \end{aligned} \quad (\text{B3})$$

where x has been defined in Eq. (A3) and $f(x)$ is given in Eq. (A4). The x integration, based on the energy conservation relation and assuming $|A_{p\bar{p}B}^{B,BC}(\mathbf{q}, k, x)|$ is independent of x and depends mainly on q , i.e., $|A_{p\bar{p}B}^{B,BC}(\mathbf{q}, \mathbf{k})| \approx |h(q)|$, gives

$$\int \delta(f(x)) |A_{p\bar{p}B}^{B,BC}(\mathbf{q}, \mathbf{k})|^2 \frac{dx}{E(-\mathbf{q} - \mathbf{k})} \approx \frac{|h(q)|^2}{qk}, \quad (\text{B4})$$

⁴One has $\lambda(x, y, z) = x^2 + y^2 + z^2 - 2xy - 2yz - 2zx = (x + y - z)^2 - 4xy = (-x + y + z)^2 - 4yz = (x - y + z)^2 - 4zx$.

where x is fixed now at the value x_0 given by Eq. (A5) with the condition $-1 \leq x_0 \leq 1$. Therefore, we have

$$\Gamma(p\bar{p}\mathcal{B}) = \frac{1}{32\pi^3 M_{J/\psi}} \int M_{p\bar{p}} dM_{p\bar{p}} \int \frac{qdq}{E(q)} |h|^2. \quad (\text{B5})$$

The experimental spectrum of the $p\bar{p}$ invariant mass is rather complicated and its description is a check for the theory in question. Since we may write the width for the emission of a vector particle as

$$\Gamma(p\bar{p}\mathcal{B}) = \int dM_{p\bar{p}} S(M_{p\bar{p}}), \quad (\text{B6})$$

where $S(M_{p\bar{p}})$ denotes the spectral function, we have

$$S(M_{p\bar{p}}) = \frac{M_{p\bar{p}}}{32\pi^3 M_{J/\psi}} \int \frac{qdq}{E(q)} |h(q)|^2 = \frac{M_{p\bar{p}}}{32\pi^3 M_{J/\psi}} \int_{E_-}^{E_+} dE |h(q)|^2, \quad (\text{B7})$$

where the integration limits E_- and E_+ are given in Eq. (A8) while the invariant mass $M_{p\bar{p}}$ is defined by Eq. (A6) and the emitted particle momentum $k(M_{p\bar{p}})$ is read from Eq. (A9). Numerical calculations at the endpoints require care and the following approximate expression is helpful to check the accuracy,

$$S(M_{p\bar{p}}) \approx \frac{M_{p\bar{p}}}{32\pi^3 M_{J/\psi}} (E_+ - E_-) |h|^2, \quad (\text{B8})$$

assuming further that $|h|^2$ depends only weakly on E . From Eq. (A8), the difference $E_+ - E_-$ is simply

$$E_+ - E_- = k(M_{p\bar{p}}) \frac{\sqrt{M_{p\bar{p}}^2 - 4m^2}}{M_{p\bar{p}}}.$$

So, finally, the spectral function reads

$$S(M_{p\bar{p}}) = \frac{\sqrt{\lambda(M_B^2, M_{J/\psi}^2, M_{p\bar{p}}^2)} [M_{p\bar{p}}^2 - 4m^2]}{64\pi^3 M_{J/\psi}^2} |h|^2 \quad (\text{B9})$$

and this formula is useful to understand the end points. Close to the $p\bar{p}$ threshold, $M_{p\bar{p}} = 2m$, one finds $S \sim \sqrt{k_M - k}$ where $k_M = (M_{J/\psi}^2 - 4m^2)/2M_{J/\psi} = 979.14$ MeV is the maximal value of k reached at the threshold. This limit leads to $k = 2q$ and the partners in the $p\bar{p}$ pair run parallel in the direction opposite to the photon direction. Such a configuration enhances final-state interactions. This dependence in $k_M - k$ determines the position of the threshold peak in S . At the other end of the spectrum, $M_{p\bar{p}} = M_{J/\psi} - m_B$, one has $S \sim k = 0$.

APPENDIX C: EXPLICIT EXPRESSIONS FOR THE ELECTROMAGNETIC OPERATORS

Let q be the initial nucleon four-momentum and $q' = q - k$ that of the nucleon after emission of the boson with four-momentum k . The following Lorentz condition applies

$$\mathbf{k} \cdot \boldsymbol{\epsilon}^*(\lambda) - k_0 \epsilon_0^*(\lambda) = 0, \quad (\text{C1})$$

which in the case of the photon leads to

$$\mathbf{k} \cdot \boldsymbol{\epsilon}^*(\lambda) = 0, \quad (\text{C2})$$

and for a massive vector particle to

$$\epsilon_0^*(\lambda) = \mathbf{k} \cdot \boldsymbol{\epsilon}^*(\lambda) / k_0. \quad (\text{C3})$$

The vector part of the current reads

$$\mathcal{A}_V(q', q, \boldsymbol{\epsilon}^*(\lambda)) = \bar{u}(q') \gamma_\mu \epsilon^{\mu*}(\lambda) u(q) = \chi_{S'}^\dagger A_V(\mathbf{q}, \mathbf{k}, \boldsymbol{\epsilon}^*(\lambda)) \chi_S, \quad (\text{C4})$$

where χ_S and $\chi_{S'}$ denote the standard two-dimensional spin vectors. The four-dimensional spinors read

$$u(q) = \sqrt{\frac{\Omega}{2m}} \begin{pmatrix} \chi_S \\ \frac{\boldsymbol{\sigma} \cdot \mathbf{q}}{\Omega} \chi_S \end{pmatrix}, \quad \bar{u}(q') = u(q')^\dagger \gamma_0 = \sqrt{\frac{\Omega'}{2m}} \begin{pmatrix} \chi_{S'}^\dagger & \frac{\boldsymbol{\sigma} \cdot \mathbf{q}'}{\Omega'} \chi_{S'}^\dagger \end{pmatrix} \gamma_0 = \sqrt{\frac{\Omega'}{2m}} \begin{pmatrix} \chi_{S'}^\dagger & -\frac{\boldsymbol{\sigma} \cdot \mathbf{q}'}{\Omega'} \chi_{S'}^\dagger \end{pmatrix}, \quad (\text{C5})$$

where the energies Ω and Ω' are

$$\Omega = m + E_q \quad \text{and} \quad \Omega' = m + \sqrt{(\mathbf{q} - \mathbf{k})^2 + m^2}, \quad (\text{C6})$$

$$E_q = \sqrt{q^2 + m^2}, \quad (\text{C7})$$

with m being the nucleon mass. In the following, we use the Bjorken and Drell definitions of the Pauli σ and γ matrices [36]. Hence, from Eq. (C4) for the vector term, we can write

$$A_V(q', q, \epsilon^*(\lambda)) = N \left[\left(1 + \frac{\boldsymbol{\sigma} \cdot \mathbf{q}'}{\Omega'} \frac{\boldsymbol{\sigma} \cdot \mathbf{q}}{\Omega} \right) \epsilon_0^*(\lambda) - \left(\frac{\boldsymbol{\sigma} \cdot \boldsymbol{\epsilon}^*(\lambda) \boldsymbol{\sigma} \cdot \mathbf{q}}{\Omega} + \frac{\boldsymbol{\sigma} \cdot \mathbf{q}' \boldsymbol{\sigma} \cdot \boldsymbol{\epsilon}^*(\lambda)}{\Omega'} \right) \right], \quad (\text{C8})$$

with the normalization factor N :

$$N = \frac{\sqrt{\Omega \Omega'}}{2m} = \frac{\Omega \zeta}{2m} \quad \text{with} \quad \zeta = \sqrt{\frac{\Omega'}{\Omega}}. \quad (\text{C9})$$

Upon using the standard relation for any two vectors \mathbf{v} and \mathbf{w} ,

$$(\boldsymbol{\sigma} \cdot \mathbf{v})(\boldsymbol{\sigma} \cdot \mathbf{w}) = \mathbf{v} \cdot \mathbf{w} + i \boldsymbol{\sigma} \cdot (\mathbf{v} \wedge \mathbf{w}), \quad (\text{C10})$$

the spin operator $A_V(\mathbf{k}, \mathbf{q}, \epsilon^*(\lambda))$ becomes

$$A_V(\mathbf{q}, \mathbf{k}, \epsilon^*(\lambda)) = \frac{\mathbf{k} \cdot \boldsymbol{\epsilon}^*(\lambda)}{2mk_0} \left\{ \Omega \zeta + \frac{\mathbf{q} \cdot (\mathbf{q} - \mathbf{k})}{\Omega \zeta} - i \frac{\boldsymbol{\sigma} \cdot (\mathbf{k} \wedge \mathbf{q})}{\Omega \zeta} \right\} - \frac{1}{2m} \left\{ \left(\zeta + \frac{1}{\zeta} \right) \mathbf{q} \cdot \boldsymbol{\epsilon}^*(\lambda) - \frac{1}{\zeta} \mathbf{k} \cdot \boldsymbol{\epsilon}^*(\lambda) - i \left(\zeta - \frac{1}{\zeta} \right) \boldsymbol{\sigma} \cdot [\mathbf{q} \wedge \boldsymbol{\epsilon}^*(\lambda)] - i \frac{1}{\zeta} \boldsymbol{\sigma} \cdot (\mathbf{k} \wedge \boldsymbol{\epsilon}^*(\lambda)) \right\}. \quad (\text{C11})$$

For the emission from the antinucleon with momentum $-\mathbf{q}$, we simply have to change in Eqs. (C11) and (C18) \mathbf{q} into $-\mathbf{q}$:

$$\bar{A}_V(\mathbf{q}, \mathbf{k}, \epsilon^*(\lambda)) = A_V(-\mathbf{q}, \mathbf{k}, \epsilon^*(\lambda)). \quad (\text{C12})$$

The substitution $\mathbf{q} \rightarrow -\mathbf{q}$ induces $\zeta \rightarrow \bar{\zeta}$ where

$$\bar{\zeta} = \sqrt{\frac{\bar{\Omega}}{\Omega}} \quad \text{with} \quad \bar{\Omega} = m + \sqrt{(\mathbf{q} + \mathbf{k})^2 + m^2}. \quad (\text{C13})$$

The tensor piece is more elaborate:

$$A_T(k, q, \epsilon^*(\lambda)) = \bar{u}(q') \sigma_{\mu\nu} k^\mu \epsilon^{\nu*}(\lambda) u(q) = \chi_S^\dagger A_T(\mathbf{k}, \mathbf{q}, \epsilon^*(\lambda)) \chi_S, \quad (\text{C14})$$

with

$$A_T(\mathbf{q}, \mathbf{k}, \epsilon^*(\lambda)) = \frac{\Omega \zeta}{2m} \left(1 - \frac{\boldsymbol{\sigma} \cdot \mathbf{q}'}{\Omega'} \right) \sigma_{\mu\nu} k^\mu \epsilon^{\nu*}(\lambda) \left(\frac{\boldsymbol{\sigma} \cdot \mathbf{q}}{\Omega} \right). \quad (\text{C15})$$

Since

$$\sigma_{\mu\nu} k^\mu \epsilon^{\nu*}(\lambda)(k) = -i k_0 \begin{pmatrix} 0 & \boldsymbol{\sigma} \cdot \boldsymbol{\epsilon}^*(\lambda) \\ \boldsymbol{\sigma} \cdot \boldsymbol{\epsilon}^*(\lambda) & 0 \end{pmatrix} + i \epsilon_0^*(\lambda) \begin{pmatrix} 0 & \boldsymbol{\sigma} \cdot \mathbf{k} \\ \boldsymbol{\sigma} \cdot \mathbf{k} & 0 \end{pmatrix} + \begin{pmatrix} \boldsymbol{\sigma} \cdot [\mathbf{k} \wedge \boldsymbol{\epsilon}^*(\lambda)] & 0 \\ 0 & \boldsymbol{\sigma} \cdot (\mathbf{k} \wedge \boldsymbol{\epsilon}^*(\lambda)) \end{pmatrix},$$

we obtain

$$A_T(\mathbf{k}, \mathbf{q}, \epsilon^*(\lambda)) = \frac{\Omega \zeta}{2m} \left\{ -i k_0 \left[\frac{\boldsymbol{\sigma} \cdot \boldsymbol{\epsilon}^*(\lambda) \boldsymbol{\sigma} \cdot \mathbf{q}}{\Omega} - \frac{\boldsymbol{\sigma} \cdot \mathbf{q}' \boldsymbol{\sigma} \cdot \boldsymbol{\epsilon}^*(\lambda)}{\Omega'} \right] + i \epsilon_0^*(\lambda) \left[\frac{\boldsymbol{\sigma} \cdot \mathbf{k} \boldsymbol{\sigma} \cdot \mathbf{q}}{\Omega} - \frac{\boldsymbol{\sigma} \cdot \mathbf{q}' \boldsymbol{\sigma} \cdot \mathbf{k}}{\Omega'} \right] + \boldsymbol{\sigma} \cdot [\mathbf{k} \wedge \boldsymbol{\epsilon}^*(\lambda)] - \frac{\boldsymbol{\sigma} \cdot \mathbf{q}'}{\Omega'} \boldsymbol{\sigma} \cdot [\mathbf{k} \wedge \boldsymbol{\epsilon}^*(\lambda)] \frac{\boldsymbol{\sigma} \cdot \mathbf{q}}{\Omega} \right\}. \quad (\text{C16})$$

With the repeated use of Eq. (C10) and of double vectorial product properties, we are led to the following explicit expression:

$$A_T(\mathbf{q}, \mathbf{k}, \epsilon^*(\lambda)) = \frac{i}{2m} \frac{\mathbf{k} \cdot \boldsymbol{\epsilon}^*(\lambda)}{k_0} \left[\left(\zeta - \frac{1}{\zeta} + \frac{k_0}{\Omega \zeta} \right) \mathbf{k} \cdot \mathbf{q} + \frac{1}{\zeta} (\mathbf{k}^2 - k_0^2) + i \left(\zeta + \frac{1}{\zeta} + \frac{k_0}{\Omega \zeta} \right) \boldsymbol{\sigma} \cdot (\mathbf{k} \wedge \mathbf{q}) \right] - \frac{i k_0}{2m} \mathbf{q} \cdot \boldsymbol{\epsilon}^*(\lambda) \left[\zeta - \frac{1}{\zeta} + \frac{\mathbf{k}^2}{k_0 \Omega \zeta} + \frac{i}{k_0 \Omega \zeta} \boldsymbol{\sigma} \cdot (\mathbf{k} \wedge \mathbf{q}) \right] + \frac{\Omega \zeta}{2m} \boldsymbol{\sigma} \cdot [\mathbf{k} \wedge \boldsymbol{\epsilon}^*(\lambda)] \left[1 + \frac{k_0}{\Omega \zeta^2} \right] - \frac{k_0}{2m} \boldsymbol{\sigma} \cdot [\mathbf{q} \wedge \boldsymbol{\epsilon}^*(\lambda)] \left[\zeta + \frac{1}{\zeta} - \frac{1}{k_0 \Omega \zeta} (\mathbf{q} - \mathbf{k}) \cdot \mathbf{k} \right] - \frac{1}{2m} \frac{1}{\Omega \zeta} \mathbf{q} \cdot [\mathbf{k} \wedge \boldsymbol{\epsilon}^*(\lambda)] \boldsymbol{\sigma} \cdot \mathbf{q}, \quad (\text{C17})$$

where $k_0 = \sqrt{\mathbf{k}^2 + m_B^2}$. The tensor amplitude for the emission from the antinucleon will be obtained from the replacements $\mathbf{q} \rightarrow -\mathbf{q}$ and hence $\zeta \rightarrow \bar{\zeta}$ in Eq. (C17).

1. The specific case of the photon

For the photon, since $\epsilon_0^*(\lambda) = 0$ and thus $\mathbf{k} \cdot \epsilon^*(\lambda) = 0$, the vector amplitude reduces to

$$A_{V,\gamma}(\mathbf{q}, \mathbf{k}, \epsilon^*(\lambda)) = -\frac{1}{2m} \left\{ \left(\zeta + \frac{1}{\zeta} \right) \mathbf{q} \cdot \epsilon^*(\lambda) - i \left(\zeta - \frac{1}{\zeta} \right) \boldsymbol{\sigma} \cdot [\mathbf{q} \wedge \epsilon^*(\lambda)] - i \frac{1}{\zeta} \boldsymbol{\sigma} \cdot [\mathbf{k} \wedge \epsilon^*(\lambda)] \right\}, \quad (\text{C18})$$

while the tensor amplitude becomes

$$A_{T,\gamma}(\mathbf{q}, \mathbf{k}, \epsilon^*(\lambda)) = -\frac{i k_0}{2m} \mathbf{q} \cdot \epsilon^*(\lambda) \left[\zeta - \frac{1}{\zeta} + \frac{\mathbf{k}^2}{k_0 \Omega \zeta} + \frac{i}{k_0 \Omega \zeta} \boldsymbol{\sigma} \cdot (\mathbf{k} \wedge \mathbf{q}) \right] + \frac{\Omega \zeta}{2m} \boldsymbol{\sigma} \cdot [\mathbf{k} \wedge \epsilon^*(\lambda)] \left[1 + \frac{k_0}{\Omega \zeta^2} \right] \\ - \frac{k_0}{2m} \boldsymbol{\sigma} \cdot [\mathbf{q} \wedge \epsilon^*(\lambda)] \left[\zeta + \frac{1}{\zeta} - \frac{1}{k_0 \Omega \zeta} (\mathbf{q} - \mathbf{k}) \cdot \mathbf{k} \right] - \frac{1}{2m} \frac{1}{\Omega \zeta} \mathbf{q} \cdot [\mathbf{k} \wedge \epsilon^*(\lambda)] \boldsymbol{\sigma} \cdot \mathbf{q}, \quad (\text{C19})$$

where, here, $k_0 = |\mathbf{k}| = k$. The corresponding photon amplitude for the antinucleon emission, $\bar{A}_{T,\gamma}$, will be obtained with the replacement $\mathbf{q} \rightarrow -\mathbf{q}$, which induces $\zeta \rightarrow \bar{\zeta}$.

The vertex coupling yields for the photon emission from the nucleon

$$V_N^\gamma(\mathbf{q}, \mathbf{k}) = e \left(A_{V,\gamma} + i \frac{\kappa}{2m} A_{T,\gamma} \right) = -\frac{e}{2m} \left\{ \left(\zeta + \frac{1}{\zeta} \right) - \frac{\kappa k_0}{2m} \left[\zeta - \frac{1}{\zeta} + \frac{k_0}{\Omega \zeta} + i \frac{\boldsymbol{\sigma} \cdot (\mathbf{k} \wedge \mathbf{q})}{k_0 \Omega \zeta} \right] \right\} \mathbf{q} \cdot \epsilon^*(\lambda) \\ + \frac{ie}{2m} \left\{ \left(\zeta - \frac{1}{\zeta} \right) - \frac{\kappa k_0}{2m} \left(\zeta + \frac{1}{\zeta} - \frac{\mathbf{q} \cdot \mathbf{k} - k_0^2}{k_0 \Omega \zeta} \right) \right\} \boldsymbol{\sigma} \cdot (\mathbf{q} \wedge \epsilon^*(\lambda)) \\ + \frac{ie}{2m} \left\{ \frac{1}{\zeta} + \frac{\kappa}{2m} \left(\Omega \zeta + \frac{k_0}{\zeta} \right) \right\} \boldsymbol{\sigma} \cdot [\mathbf{k} \wedge \epsilon^*(\lambda)] - \frac{ie\kappa}{2m} \frac{\mathbf{q} \cdot [\mathbf{k} \wedge \epsilon^*(\lambda)]}{2m\Omega \zeta} \boldsymbol{\sigma} \cdot \mathbf{q}, \quad (\text{C20})$$

and correspondingly for the emission from the antinucleon

$$V_{\bar{N}}^\gamma(\mathbf{q}, \mathbf{k}) = -e \left[\bar{A}_{V,\gamma}(-\mathbf{q}, \mathbf{k}) + i \frac{\kappa}{2m} \bar{A}_{T,\gamma}(-\mathbf{q}, \mathbf{k}) \right] \quad (\text{C21})$$

obtained by making the substitutions, $e \rightarrow -e$, $\mathbf{q} \rightarrow -\mathbf{q}$ and, hence, $\zeta \rightarrow \bar{\zeta}$.

Labeling the nucleon part by 1 and the antinucleon part by 2, we will get the potential for the photon emission, and recombining these expressions gives

$$U_\gamma^0(\mathbf{q}, \mathbf{k}) = \frac{e}{2m} \left\{ f(\mathbf{q}, \mathbf{k}) + \bar{f}(\mathbf{q}, \mathbf{k}) + i \frac{\kappa}{2m\Omega} \left(\frac{\boldsymbol{\sigma}_1}{\zeta} - \frac{\boldsymbol{\sigma}_2}{\bar{\zeta}} \right) \cdot (\mathbf{k} \wedge \mathbf{q}) \right\} \mathbf{q} \cdot \epsilon^*(\lambda) \\ + \frac{ie}{2m} \left[g(\mathbf{q}, \mathbf{k}) \boldsymbol{\sigma}_1 + \bar{g}(\mathbf{q}, \mathbf{k}) \boldsymbol{\sigma}_2 + \frac{\kappa}{2m\Omega} \mathbf{q} \cdot \mathbf{k} \left\{ \frac{\boldsymbol{\sigma}_1}{\zeta} - \frac{\boldsymbol{\sigma}_2}{\bar{\zeta}} \right\} \right] \cdot [\mathbf{q} \wedge \epsilon^*(\lambda)] \\ + \frac{ie}{2m} [h(\mathbf{q}, \mathbf{k}) \boldsymbol{\sigma}_1 - \bar{h}(\mathbf{q}, \mathbf{k}) \boldsymbol{\sigma}_2] \cdot [\mathbf{k} \wedge \epsilon^*(\lambda)] - \frac{ie\kappa}{2m} \frac{\mathbf{q} \cdot [\mathbf{k} \wedge \epsilon^*(\lambda)]}{2m\Omega} \left(\frac{\boldsymbol{\sigma}_1}{\zeta} - \frac{\boldsymbol{\sigma}_2}{\bar{\zeta}} \right) \cdot \mathbf{q}, \quad (\text{C22})$$

where we have introduced

$$f(\mathbf{q}, \mathbf{k}) = -\left(\zeta + \frac{1}{\zeta} \right) + \frac{k\kappa}{2m} \left(\zeta - \frac{1}{\zeta} + \frac{k}{\Omega \zeta} \right), \quad g(\mathbf{q}, \mathbf{k}) = \left(\zeta - \frac{1}{\zeta} \right) - \frac{k\kappa}{2m} \left(\zeta + \frac{1}{\zeta} + \frac{k}{\Omega \zeta} \right), \quad h(\mathbf{q}, \mathbf{k}) = \frac{1}{\zeta} + \frac{k\kappa}{2m} \left(\frac{\Omega \zeta}{k} + \frac{1}{\zeta} \right), \quad (\text{C23})$$

where we have used $k = k_0$. The bar functions are identical but with $\zeta \rightarrow \bar{\zeta}$.

2. The case for the ω meson

For completeness, we present below the exact expressions for the ω meson emission. Only a few terms are really exploited in the present work. With

$$k_0 = E_\omega = \sqrt{\mathbf{k}^2 + m_\omega^2}, \quad (\text{C24})$$

where m_ω denotes the mass of the ω meson, and, taking into account the change of sign of the ω coupling at the \bar{N} vertex because of G parity, from Eqs. (38) and (C8), the vector piece will read

$$A_{V,\omega} = g_{V\omega} \frac{\mathbf{k} \cdot \epsilon^*(\lambda)}{2mE_\omega} \left[\Omega(\zeta - \bar{\zeta}) + \frac{\mathbf{q}^2}{\Omega} \left(\frac{1}{\zeta} - \frac{1}{\bar{\zeta}} \right) - \frac{\mathbf{k} \cdot \mathbf{q}}{\Omega} \left(\frac{1}{\zeta} + \frac{1}{\bar{\zeta}} \right) - i \frac{1}{\Omega} \left(\frac{\boldsymbol{\sigma}_1}{\zeta} + \frac{\boldsymbol{\sigma}_2}{\bar{\zeta}} \right) \cdot (\mathbf{k} \wedge \mathbf{q}) \right]$$

$$\begin{aligned}
& -\frac{g_{V\omega}}{2m} \left[\left(\zeta + \frac{1}{\zeta} + \bar{\zeta} + \frac{1}{\bar{\zeta}} \right) \mathbf{q} \cdot \boldsymbol{\epsilon}^*(\lambda) - \left(\frac{1}{\zeta} - \frac{1}{\bar{\zeta}} \right) \mathbf{k} \cdot \boldsymbol{\epsilon}^*(\lambda) \right. \\
& \left. - i \left(\frac{\boldsymbol{\sigma}_1}{\zeta} - \frac{\boldsymbol{\sigma}_2}{\bar{\zeta}} \right) \cdot [\mathbf{k} \wedge \boldsymbol{\epsilon}^*(\lambda)] - i \left\{ \left(\zeta - \frac{1}{\zeta} \right) \boldsymbol{\sigma}_1 + \left(\bar{\zeta} - \frac{1}{\bar{\zeta}} \right) \boldsymbol{\sigma}_2 \right\} \cdot \{\mathbf{q} \wedge \boldsymbol{\epsilon}^*(\lambda)\} \right], \tag{C25}
\end{aligned}$$

which to order $k^2/4m^2$ reduces to

$$\begin{aligned}
A_{V,\omega} \approx & \frac{g_{V\omega}}{2m} \left[2 \left(-1 + \frac{q^2}{2\Omega E_q} - \frac{\Omega}{2E_q} \right) \frac{\mathbf{k} \cdot \mathbf{q}}{\Omega} - \frac{i}{\Omega} (\boldsymbol{\sigma}_1 + \boldsymbol{\sigma}_2) \cdot (\mathbf{k} \wedge \mathbf{q}) \right] \frac{\mathbf{k} \cdot \boldsymbol{\epsilon}^*(\lambda)}{E_\omega} \\
& - \frac{g_{V\omega}}{2m} \left\{ 4 \mathbf{q} \cdot \boldsymbol{\epsilon}^*(\lambda) - i (\boldsymbol{\sigma}_1 - \boldsymbol{\sigma}_2) \cdot [\mathbf{k} \wedge \boldsymbol{\epsilon}^*(\lambda)] + i \frac{\mathbf{k} \cdot \mathbf{q}}{\Omega E_q} (\boldsymbol{\sigma}_1 - \boldsymbol{\sigma}_2) \cdot [\mathbf{q} \wedge \boldsymbol{\epsilon}^*(\lambda)] \right\}, \tag{C26}
\end{aligned}$$

where E_q has been defined in Eq. (C7) and Ω in Eq. (C6). Then we have to add the tensor piece, knowing that the coupling constant for this part is rather ill known but most likely small:

$$\begin{aligned}
E_\omega A_{T,\omega} = & i \frac{g_{T\omega}}{2m} \left\{ i \left[\zeta + \bar{\zeta} - \left(1 - \frac{E_\omega}{\Omega} \right) \left(\frac{1}{\zeta} + \frac{1}{\bar{\zeta}} \right) \right] \mathbf{k} \cdot \mathbf{q} + \left(\frac{1}{\zeta} - \frac{1}{\bar{\zeta}} \right) (\mathbf{k}^2 - E_\omega^2) \right. \\
& + i (\zeta \boldsymbol{\sigma}_1 + \bar{\zeta} \boldsymbol{\sigma}_2) \cdot (\mathbf{k} \wedge \mathbf{q}) + i \left(1 + \frac{E_\omega}{\Omega} \right) \left(\frac{\boldsymbol{\sigma}_1}{\zeta} + \frac{\boldsymbol{\sigma}_2}{\bar{\zeta}} \right) \cdot (\mathbf{k} \wedge \mathbf{q}) \left. \right\} \frac{\mathbf{k} \cdot \boldsymbol{\epsilon}^*(\lambda)}{2m E_\omega} \\
& - i \frac{E_\omega}{2m} \left[\left[\zeta + \bar{\zeta} - \left(1 - \frac{k^2}{E_\omega \Omega} \right) \left(\frac{1}{\zeta} + \frac{1}{\bar{\zeta}} \right) \right] + \frac{i}{E_\omega \Omega} \left(\frac{\boldsymbol{\sigma}_1}{\zeta} - \frac{\boldsymbol{\sigma}_2}{\bar{\zeta}} \right) \cdot (\mathbf{k} \wedge \mathbf{q}) \right] \mathbf{q} \cdot \boldsymbol{\epsilon}^*(\lambda) \\
& + \frac{\Omega}{2m} \left[\left(\zeta + \frac{E_\omega}{\Omega \zeta} \right) \boldsymbol{\sigma}_1 - \left(\bar{\zeta} + \frac{E_\omega}{\Omega \bar{\zeta}} \right) \boldsymbol{\sigma}_2 \right] \cdot [\mathbf{k} \wedge \boldsymbol{\epsilon}^*(\lambda)] - \frac{E_\omega}{2m} \left[\left(\zeta + \frac{1}{\zeta} + \frac{E_\omega}{\Omega \zeta} - \frac{\mathbf{k} \cdot \mathbf{q}}{E_\omega \Omega \zeta} \right) \boldsymbol{\sigma}_1 \right. \\
& \left. + \left(\bar{\zeta} + \frac{1}{\bar{\zeta}} + \frac{k^2}{E_\omega \Omega \bar{\zeta}} + \frac{\mathbf{k} \cdot \mathbf{q}}{E_\omega \Omega \bar{\zeta}} \right) \boldsymbol{\sigma}_2 \right] \cdot [\mathbf{q} \wedge \boldsymbol{\epsilon}^*(\lambda)] - \frac{\mathbf{q} \cdot [\mathbf{k} \wedge \boldsymbol{\epsilon}^*(\lambda)]}{2m \Omega} \left(\frac{\boldsymbol{\sigma}_1}{\zeta} - \frac{\boldsymbol{\sigma}_2}{\bar{\zeta}} \right) \cdot \mathbf{q} \left. \right\}. \tag{C27}
\end{aligned}$$

We have then

$$V_\omega = A_{V,\omega} + A_{T,\omega}. \tag{C28}$$

APPENDIX D: AMPLITUDES FOR BOSON EMISSION

The boson with 3-momentum \mathbf{k} is emitted either from the nucleon (labeled 1) or from the antinucleon (labeled 2) lines. In the rest frame of the J/ψ , the nucleon momentum prior to the photon emission is denoted \mathbf{q} and $-\mathbf{q}$ is that of the antinucleon. The mass of the nucleon and antinucleon is denoted by m . The various variables that occur in this appendix, Ω , Ω' , $\bar{\Omega}$, ζ , and $\bar{\zeta}$, are given in Eqs. (C6), (C9), and (C13).

1. Photon emission

a. Vector coupling

When the photon is emitted from the nucleon line, the contribution of the vector term to the amplitude is given by Eq. (C18) multiplied by the charge e and where the helicity λ takes the values ± 1 . To obtain the amplitude corresponding to the photon emission from the antinucleon line, one has simply to substitute $e \rightarrow -e$ and $\mathbf{q} \rightarrow -\mathbf{q}$. Thus, the full amplitude arising from the vector coupling reads

$$\bar{A}_V(\mathbf{q}, \mathbf{k}, \boldsymbol{\epsilon}^*(\lambda)) = \bar{A}_{V,a}^\gamma + \bar{A}_{V,b}^\gamma + \bar{A}_{V,c}^\gamma, \tag{D1}$$

with

$$\bar{A}_{V,a}^\gamma(\mathbf{q}, \mathbf{k}, \boldsymbol{\epsilon}^*(\lambda)) = -\frac{e}{2m} \left[\left(\zeta + \frac{1}{\zeta} \right) + \left(\bar{\zeta} + \frac{1}{\bar{\zeta}} \right) \right] \mathbf{q} \cdot \boldsymbol{\epsilon}^*(\lambda), \tag{D2}$$

$$\bar{A}_{V,b}^\gamma(\mathbf{q}, \mathbf{k}, \boldsymbol{\epsilon}^*(\lambda)) = \frac{ie}{2m} \left[\left(\zeta - \frac{1}{\zeta} \right) \boldsymbol{\sigma}_1 \cdot \mathbf{q} \wedge \boldsymbol{\epsilon}^*(\lambda) + \left(\bar{\zeta} - \frac{1}{\bar{\zeta}} \right) \boldsymbol{\sigma}_2 \cdot \mathbf{q} \wedge \boldsymbol{\epsilon}^*(\lambda) \right], \tag{D3}$$

$$\bar{A}_{V,c}^\gamma(\mathbf{q}, \mathbf{k}, \boldsymbol{\epsilon}^*(\lambda)) = \frac{ie}{2m} \left(\frac{\boldsymbol{\sigma}_1}{\zeta} - \frac{\boldsymbol{\sigma}_2}{\bar{\zeta}} \right) \cdot \mathbf{k} \wedge \boldsymbol{\epsilon}^*(\lambda). \tag{D4}$$

In these equations $\lambda = \pm 1$ and since, for the photon, $\epsilon_0^*(\lambda) = 0$ and \mathbf{k} is chosen to lie along the z axis, the orthogonality relation $\mathbf{k} \cdot \boldsymbol{\epsilon}^*(\lambda) = 0$ implies

$$\boldsymbol{\epsilon}^*(\lambda = \pm 1) = \frac{1}{\sqrt{2}}(-\lambda, -i, 0). \quad (\text{D5})$$

The $\bar{A}_{V,a}^\gamma$ amplitude contributes to the ${}^3S_1 \rightarrow {}^3P_1$ electric coupling amplitude (D19). The $\bar{A}_{V,b}^\gamma$ amplitude leads to a final 3P_0 state not included, so far, in our work. Note that it vanishes in the approximation $\zeta \sim \bar{\zeta}$. The $\bar{A}_{V,c}^\gamma$ amplitude contributes to the ${}^3S_1 \rightarrow {}^1S_0$ transition.

b. Tensor coupling

With the same notations as above, the exact amplitude for the tensor coupling when the photon is emitted from the nucleon line reads

$$A_1^\gamma(\mathbf{q}, \mathbf{k}, \boldsymbol{\epsilon}^*(\lambda)) = \frac{e\kappa_N}{4m^2} \left\{ k \mathbf{q} \cdot \boldsymbol{\epsilon}^*(\lambda) \left(\zeta - \frac{1}{\zeta} + \frac{k}{\Omega\zeta} + \frac{i}{k\Omega\zeta} \boldsymbol{\sigma}_1 \cdot \mathbf{k} \wedge \mathbf{q} \right) + i \boldsymbol{\sigma}_1 \cdot \mathbf{k} \wedge \boldsymbol{\epsilon}^*(\lambda) \left(\Omega\zeta + \frac{k}{\zeta} \right) - ik \boldsymbol{\sigma}_1 \cdot \mathbf{q} \wedge \boldsymbol{\epsilon}^*(\lambda) \left[\zeta + \frac{1}{\zeta} - \frac{1}{k\Omega\zeta} (\mathbf{q} - \mathbf{k}) \cdot \mathbf{k} \right] - \frac{i}{\Omega\zeta} \mathbf{q} \cdot [\mathbf{k} \wedge \boldsymbol{\epsilon}^*(\lambda)] \boldsymbol{\sigma}_1 \cdot \mathbf{q} \right\}, \quad (\text{D6})$$

where κ_N is either κ_p or κ_n . In the following, we do not keep the terms proportional to $\boldsymbol{\sigma}_1 \cdot \mathbf{q} \wedge \boldsymbol{\epsilon}^*(\lambda)$ and depending on q^2 as they will contribute to final 3P_0 and D waves, respectively. These P and D wave are absent in our model. Thus, the amplitude is reduced to

$$A_1^\gamma(\mathbf{q}, \mathbf{k}, \boldsymbol{\epsilon}^*(\lambda)) \approx \frac{e\kappa_N}{4m^2} \left\{ k \mathbf{q} \cdot \boldsymbol{\epsilon}^*(\lambda) \left(\zeta - \frac{1}{\zeta} + \frac{k}{\Omega\zeta} \right) + i \boldsymbol{\sigma}_1 \cdot \mathbf{k} \wedge \boldsymbol{\epsilon}^*(\lambda) \left(\Omega\zeta + \frac{k}{\zeta} \right) \right\}, \quad (\text{D7})$$

to which we have to add the part associated to the emission from the antinucleon $A_2^\gamma(\mathbf{q}, \mathbf{k}, \boldsymbol{\epsilon}^*(\lambda))$. Thus the total tensor amplitude in this approximation $A_T^\gamma(\mathbf{q}, \mathbf{k}, \boldsymbol{\epsilon}^*(\lambda))$ can be split into two contributions (with $\lambda = \pm 1$):

$$A_T^\gamma(\mathbf{q}, \mathbf{k}, \boldsymbol{\epsilon}^*(\lambda)) = A_1^\gamma(\mathbf{q}, \mathbf{k}, \boldsymbol{\epsilon}^*(\lambda)) + A_2^\gamma(\mathbf{q}, \mathbf{k}, \boldsymbol{\epsilon}^*(\lambda)) = A_{T,a}^\gamma(\mathbf{q}, \mathbf{k}, \boldsymbol{\epsilon}^*(\lambda)) + A_{T,b}^\gamma(\mathbf{q}, \mathbf{k}, \boldsymbol{\epsilon}^*(\lambda)), \quad (\text{D8})$$

with

$$A_{T,a}^\gamma(\mathbf{q}, \mathbf{k}, \boldsymbol{\epsilon}^*(\lambda)) = \frac{e\kappa_N}{4m^2} k \left[\zeta + \bar{\zeta} + \left(\frac{1}{\zeta} + \frac{1}{\bar{\zeta}} \right) \left(\frac{k}{\Omega} - 1 \right) \right] \mathbf{q} \cdot \boldsymbol{\epsilon}^*(\lambda), \quad (\text{D9})$$

and

$$A_{T,b}^\gamma(\mathbf{q}, \mathbf{k}, \boldsymbol{\epsilon}^*(\lambda)) = \frac{e\kappa_N}{4m^2} \left[i \boldsymbol{\sigma}_1 \cdot \mathbf{k} \wedge \boldsymbol{\epsilon}^*(\lambda) \left(\Omega\zeta + \frac{k}{\zeta} \right) - i \boldsymbol{\sigma}_2 \cdot \mathbf{k} \wedge \boldsymbol{\epsilon}^*(\lambda) \left(\Omega\bar{\zeta} + \frac{k}{\bar{\zeta}} \right) \right]. \quad (\text{D10})$$

The amplitude (D9) will add up to the $\bar{A}_{V,a}^\gamma(\mathbf{q}, \mathbf{k}, \boldsymbol{\epsilon}^*(\lambda))$ term (D2) to give the ${}^3S_1 \rightarrow {}^3P_1$ transition amplitude while the (D10) together with the (D4) amplitude will contribute to the ${}^3S_1 \rightarrow {}^1S_0$ transition.

c. Magnetic and electric transitions

a. ${}^3S_1 \rightarrow {}^1S_0$ transitions. The ${}^3S_1 \rightarrow {}^1S_0$ magnetic coupling amplitude will be given by the sum of the (D4) and (D10) amplitudes. For any vector \mathbf{a} , the spin matrix elements read

$$\langle {}^1S_0 | \boldsymbol{\sigma}_1 \cdot \mathbf{a} | {}^3S_1 \rangle = -\langle {}^1S_0 | \boldsymbol{\sigma}_2 \cdot \mathbf{a} | {}^3S_1 \rangle = \frac{1}{\sqrt{3}} (-i\sqrt{2}a_y + a_z), \quad (\text{D11})$$

since the spin contents of the 1S_0 and 3S_1 states are, with $|+\rangle$ the $1/2$ and $|-\rangle$ the $-1/2$ spin states, respectively,

$$|{}^1S_0\rangle = \frac{1}{\sqrt{2}} [|+\rangle - |-\rangle], \quad |{}^3S_1\rangle = \frac{1}{\sqrt{3}} \left[|+\rangle + \frac{1}{\sqrt{2}} \{ |+\rangle - |-\rangle \} + |-\rangle \right]. \quad (\text{D12})$$

With \mathbf{k} along the z axis, as already defined, we have (see Ref. [37], p. 62)

$$\boldsymbol{\epsilon}^*(\lambda = \pm 1) = \left(-\frac{\lambda}{\sqrt{2}}, -\frac{i}{\sqrt{2}}, 0 \right), \quad \mathbf{k} \wedge \boldsymbol{\epsilon}^*(\lambda = \pm 1) = \left(\frac{ik}{\sqrt{2}}, -\frac{\lambda k}{\sqrt{2}}, 0 \right), \quad (\text{D13})$$

and therefore

$$V_M^\gamma(\mathbf{q}, \mathbf{k}, \boldsymbol{\epsilon}^*(\lambda)) = \langle {}^1S_0 | [\bar{A}_{V,c}^\gamma(\mathbf{q}, \mathbf{k}, \boldsymbol{\epsilon}^*(\lambda)) + A_{T,b}^\gamma(\mathbf{q}, \mathbf{k}, \boldsymbol{\epsilon}^*(\lambda))] | {}^3S_1 \rangle = -\frac{e\lambda k}{2m\sqrt{3}} \left\{ \left(1 + \frac{\kappa_N k}{2m} \right) \left[\frac{1}{\zeta} + \frac{1}{\bar{\zeta}} \right] + \frac{\kappa_N \Omega}{2m} (\zeta + \bar{\zeta}) \right\}. \quad (\text{D14})$$

Upon summing over λ the modulus squared we get

$$\sum_{\lambda=\pm 1} |V_M^\gamma(\mathbf{q}, \mathbf{k}, \boldsymbol{\epsilon}^*(\lambda))|^2 = \frac{e^2}{4m^2} \frac{2k^2}{3} \left\{ \left(1 + \frac{\kappa_N k}{2m} \right) \left[\frac{1}{\zeta} + \frac{1}{\bar{\zeta}} \right] + \frac{\kappa_N \Omega}{2m} (\zeta + \bar{\zeta}) \right\}^2. \quad (\text{D15})$$

Note that in the small $k/2m$ limit, this reduces to

$$\sum_{\lambda=\pm 1} |V_M^\gamma(\mathbf{q}, \mathbf{k}, \boldsymbol{\epsilon}^*(\lambda))|^2 \approx \frac{8e^2}{3} \frac{k^2}{4m^2} \left[1 + \frac{\kappa_N \Omega}{2m} \right]^2, \quad (\text{D16})$$

a small contribution indeed. Using only the vector piece of the amplitude, one would have obtained

$$\frac{e^2}{4m^2} \sum_{\lambda=\pm 1} \left| \langle {}^1S_0 | \left(\frac{\boldsymbol{\sigma}_1}{\zeta} - \frac{\boldsymbol{\sigma}_2}{\bar{\zeta}} \right) \cdot \mathbf{k} \wedge \boldsymbol{\epsilon}^*(\lambda) | {}^3S_1 \rangle \right|^2 = \frac{2e^2}{3} \frac{k^2}{4m^2} \left[\frac{1}{\zeta} + \frac{1}{\bar{\zeta}} \right]^2. \quad (\text{D17})$$

Considering the final-state scattering contributions with intermediate $p\bar{p}$ and $n\bar{n}$ states (30), one obtains the following magnetic amplitude

$$V_M^\gamma(\mathbf{q}, \mathbf{k}, \boldsymbol{\epsilon}^*(\lambda)) = -\frac{\lambda e k}{4m\sqrt{3}} \left\{ \left(\frac{1}{\zeta} + \frac{1}{\bar{\zeta}} \right) (T_0 + T_1) + \frac{1}{2m} \left[\Omega(\zeta + \bar{\zeta}) + k \left(\frac{1}{\zeta} + \frac{1}{\bar{\zeta}} \right) \right] [T_0(\kappa_p + \kappa_n) + T_1(\kappa_p - \kappa_n)] \right\}, \quad (\text{D18})$$

where $T_{0,1}$ are the $N\bar{N}$ scattering amplitudes in the corresponding $I = 0, 1$ isospin states.

${}^3S_1 \rightarrow {}^3P_1$ transitions

The ${}^3S_1 \rightarrow {}^3P_1$ electric coupling amplitude is given by the sum of the amplitudes (D2) and (D9):

$$\bar{A}_{V,a}^\gamma(\mathbf{q}, \mathbf{k}, \boldsymbol{\epsilon}^*(\lambda)) + A_{T,a}^\gamma(\mathbf{q}, \mathbf{k}, \boldsymbol{\epsilon}^*(\lambda)) = -\frac{e}{2m} \mathbf{q} \cdot \boldsymbol{\epsilon}^*(\lambda) \left\{ \zeta + \frac{1}{\zeta} + \bar{\zeta} + \frac{1}{\bar{\zeta}} - \frac{k\kappa_p}{2m} \left[\zeta + \bar{\zeta} + \left(\frac{1}{\zeta} + \frac{1}{\bar{\zeta}} \right) \left(\frac{k}{\Omega} - 1 \right) \right] \right\}. \quad (\text{D19})$$

Summing the squared $\mathbf{q} \cdot \boldsymbol{\epsilon}^*(\lambda)$ term over λ gives

$$\sum_{\lambda=\pm 1} |\mathbf{q} \cdot \boldsymbol{\epsilon}^*(\lambda)|^2 = \frac{1}{2} \sum_{\lambda=\pm 1} |(-\lambda q_x + i q_y)|^2 = q^2 [1 - \cos^2 \theta_q], \quad (\text{D20})$$

where

$$\cos \theta_q = \frac{\mathbf{k} \cdot \mathbf{q}}{k q}. \quad (\text{D21})$$

Hence

$$\sum_{\lambda=\pm 1} |\bar{A}_{V,a}^\gamma(\mathbf{q}, \mathbf{k}, \boldsymbol{\epsilon}^*(\lambda)) + A_{T,a}^\gamma(\mathbf{q}, \mathbf{k}, \boldsymbol{\epsilon}^*(\lambda))|^2 = \frac{e^2 q^2}{4m^2} [1 - \cos^2 \theta_q] \left\{ \zeta + \frac{1}{\zeta} + \bar{\zeta} + \frac{1}{\bar{\zeta}} - \frac{k\kappa_p}{2m} \left[\zeta + \bar{\zeta} + \left(\frac{1}{\zeta} + \frac{1}{\bar{\zeta}} \right) \left(\frac{k}{\Omega} - 1 \right) \right] \right\}^2, \quad (\text{D22})$$

which in the small $k/2m$ limit reduces to

$$\frac{4e^2 q^2}{m^2} [1 - \cos^2 \theta_q].$$

2. ω emission

For the ω meson, the polarization vector reads (see Ref. [37], p. 62)

$$\boldsymbol{\epsilon}^*(\lambda = \pm 1) = \frac{1}{\sqrt{2}}(0, -\lambda, -i, 0), \quad \boldsymbol{\epsilon}^*(\lambda = 0) = \frac{1}{m_\omega}(k, 0, 0, E_\omega). \quad (\text{D23})$$

As before, the momentum of the emitted ω meson is assumed to lie along the z axis, so that one has

$$\mathbf{k} \cdot \boldsymbol{\epsilon}^*(\lambda = \pm 1) = 0, \quad \mathbf{k} \cdot \boldsymbol{\epsilon}^*(\lambda = 0) = \frac{k E_\omega}{m_\omega}, \quad \mathbf{k} \wedge \boldsymbol{\epsilon}^*(\lambda = \pm 1) = \frac{k}{\sqrt{2}}(i, -\lambda, 0), \quad \text{and} \quad \mathbf{k} \wedge \boldsymbol{\epsilon}^*(\lambda = 0) = 0. \quad (\text{D24})$$

The Lorentz condition, $k^\mu \cdot \boldsymbol{\epsilon}^*(\lambda)_\mu = E_\omega \boldsymbol{\epsilon}_0^*(\lambda) - \mathbf{k} \cdot \boldsymbol{\epsilon}^*(\lambda) = 0$, implies

$$\boldsymbol{\epsilon}_0^*(\lambda) = \frac{\mathbf{k} \cdot \boldsymbol{\epsilon}^*(\lambda)}{E_\omega}. \quad (\text{D25})$$

Because ω tensor coupling is small, we shall neglect its contribution [27]. If the ω is emitted from the nucleon line, the exact amplitude for the vector coupling is given by Eq. (C11) multiplied by the coupling constant $g_{V\omega}$. To obtain the full amplitude,

one has to add the amplitude corresponding to the ω emission from the antinucleon given by Eq. (C12). It is given by Eq. (C25). In addition to Eq. (D11), we have, for any vector \mathbf{a} , the equality

$$\langle {}^3P_1 | \boldsymbol{\sigma}_1 \cdot \mathbf{a} | {}^3S_1 \rangle = \langle {}^3P_1 | \boldsymbol{\sigma}_2 \cdot \mathbf{a} | {}^3S_1 \rangle. \quad (\text{D26})$$

The dominant electric contribution for $\lambda = \pm 1$ will then read

$$V_E^\omega(\lambda = \pm 1) = -\frac{g_{V\omega}}{2m} \mathbf{q} \cdot \boldsymbol{\epsilon}^*(\lambda = \pm 1) \left(\zeta + \frac{1}{\zeta} + \bar{\zeta} + \frac{1}{\bar{\zeta}} \right), \quad (\text{D27})$$

while for $\lambda = 0$, since $\epsilon_0^*(\lambda = 0) = k/m_\omega$, one has

$$V_E^\omega(\lambda = 0) = -\frac{g_{V\omega}}{2m} \left\{ \mathbf{q} \cdot \boldsymbol{\epsilon}^*(\lambda = 0) \left(\zeta + \frac{1}{\zeta} + \bar{\zeta} + \frac{1}{\bar{\zeta}} \right) + \frac{k}{m_\omega} \left[\frac{1}{\zeta} + \frac{1}{\bar{\zeta}} \right] \frac{\mathbf{k} \cdot \mathbf{q}}{\Omega} \right\}, \quad (\text{D28})$$

and, thus,

$$V_E^\omega(\lambda = 0) = -g_{V\omega} \frac{q \cos \theta_q}{2mm_\omega} \left\{ E_\omega \left(\zeta + \frac{1}{\zeta} + \bar{\zeta} + \frac{1}{\bar{\zeta}} \right) + \frac{k^2}{\Omega} \left[\frac{1}{\zeta} + \frac{1}{\bar{\zeta}} \right] \right\}. \quad (\text{D29})$$

This contributes to the ${}^3S_1 \rightarrow {}^3P_1$ transition. Summing over the helicity λ the squared amplitudes, we obtain

$$\sum_{\lambda=-1}^1 |V_E^\omega(\lambda)|^2 = g_{V\omega}^2 \frac{q^2}{4m^2} \left\{ (1 - \cos^2 \theta_q) \left[\zeta + \frac{1}{\zeta} + \bar{\zeta} + \frac{1}{\bar{\zeta}} \right]^2 + \cos^2 \theta_q \left[\frac{E_\omega}{m_\omega} \left(\zeta + \frac{1}{\zeta} + \bar{\zeta} + \frac{1}{\bar{\zeta}} \right) + \frac{k^2}{m_\omega \Omega} \left(\frac{1}{\zeta} + \frac{1}{\bar{\zeta}} \right) \right]^2 \right\}. \quad (\text{D30})$$

In the small $k/2m$ limit, this reduces to

$$\sum_{\lambda=-1}^1 |V_E^\omega(\lambda)|^2 \approx g_{V\omega}^2 \frac{4q^2}{m^2} \left\{ (1 - \cos^2 \theta_q) + \left(\frac{E_\omega}{m_\omega} \right)^2 \cos^2 \theta_q \left[1 + \frac{k^2}{E_\omega \Omega} \right] \right\},$$

giving rise again to a very small correction to the dominant piece $4g_{V\omega}^2 q^2/m^2$.

For the magnetic contribution, using Eqs. (D24) and (C25) we retain the dominant piece and get

$$V_M^\omega(\lambda = \pm 1) = i \frac{g_{V\omega}}{2m} \left\{ \frac{\boldsymbol{\sigma}_1}{\zeta} - \frac{\boldsymbol{\sigma}_2}{\bar{\zeta}} \right\} \cdot [\mathbf{k} \wedge \boldsymbol{\epsilon}^*(\lambda = \pm 1)]. \quad (\text{D31})$$

It is null for $\lambda = 0$. Then, let us thus look at the ${}^3S_1 \rightarrow {}^1S_0$ magnetic transition using Eqs. (D12):

$$\langle {}^1S_0 | V_M^\omega(\lambda = \pm 1) | {}^3S_1 \rangle = i \frac{g_{V\omega}}{2m} \langle {}^1S_0 | \left\{ \frac{\boldsymbol{\sigma}_1}{\zeta} - \frac{\boldsymbol{\sigma}_2}{\bar{\zeta}} \right\} \cdot [\mathbf{k} \wedge \boldsymbol{\epsilon}^*(\lambda = \pm 1)] | {}^3S_1 \rangle = -\frac{\lambda g_{V\omega} k}{2m\sqrt{3}} \left(\frac{1}{\zeta} + \frac{1}{\bar{\zeta}} \right). \quad (\text{D32})$$

Summing over the helicities the amplitude squared, one gets

$$\sum_{\lambda=\pm 1} |\langle {}^1S_0 | V_M^\omega(\lambda = \pm 1) | {}^3S_1 \rangle|^2 = \frac{g_{V\omega}^2}{4m^2} \frac{2k^2}{3} \left(\frac{1}{\zeta} + \frac{1}{\bar{\zeta}} \right)^2, \quad (\text{D33})$$

and thus about

$$\frac{8g_{V\omega}^2}{3} \frac{k^2}{4m^2}$$

in the small $k/2m$ limit, i.e., a very small contribution. Because the J/ψ and the ω are isospin 0 states, only the $I = 0$ component of the $p\bar{p} \rightarrow p\bar{p}$ and $n\bar{n} \rightarrow p\bar{p}$ rescattering terms contributes. In the Paris potential, the modulus of these two components being equal, there will be a cancellation either in the convention given by the Eqs. (22) and (23) of Ref. [8] or in that of Eqs. (49) and (50) [there, one will have to change the sign of the Paris $n\bar{n} \rightarrow p\bar{p}$ amplitude].

APPENDIX E: NUMERICAL CALCULATION OF THE LOOP INTEGRALS

In this appendix, we outline the numerical calculation of the loop integrals in Eqs. (31) or (59) with propagators (32) and (28). The structure of these equations is

$$I(\mathbf{q}, \mathbf{k}) = \int \frac{d\mathbf{q}'}{(2\pi)^3} T_{N\bar{N}}(\mathbf{q} - \mathbf{k}/2, \mathbf{q}' - \mathbf{k}/2, E_{N\bar{N}}) G_{0, N\bar{N}B}^+(\mathbf{q}', \mathbf{k}) \tilde{G}_{p\bar{p}}(q') U^0(\mathbf{q}', \mathbf{k}), \quad (\text{E1})$$

where we will use the half off-shell values of the $N\bar{N}$ scattering matrix evaluated from the Paris potential.

With \mathbf{k} along the z axis, \mathbf{q} in the x - z plane, and $\mathbf{q} = (q \sin \theta_q, 0, q \cos \theta_q)$, we have

$$\mathbf{q} \cdot \mathbf{q}' = qq' (\sin \theta_q \sin \theta' \cos \varphi' + \cos \theta_q \cos \theta') \quad \text{and} \quad \mathbf{k} \cdot \mathbf{q}' = kq' \cos \theta'. \quad (\text{E2})$$

Let us assume that the half off-shell dependence of the scattering matrix depends on the momentum transfer

$$T_{N\bar{N}}(\mathbf{q} - \mathbf{k}/2, \mathbf{q}' - \mathbf{k}/2, E_{N\bar{N}}) = T_{N\bar{N}}(\chi', E_{N\bar{N}}), \quad (\text{E3})$$

with

$$\chi' = \left(\mathbf{q} - \frac{\mathbf{k}}{2} \right) - \left(\mathbf{q}' - \frac{\mathbf{k}}{2} \right) = \mathbf{q} - \mathbf{q}' \quad \text{so that} \quad \chi' = \sqrt{q^2 + q'^2 - 2qq' (\sin \theta_q \sin \theta' \cos \varphi' + \cos \theta_q \cos \theta')}. \quad (\text{E4})$$

Then,

$$G_{0,N\bar{N}B}^+(\mathbf{q}', \mathbf{k}) = \frac{1}{M_{J/\psi} + i\epsilon - E_B(k) - \sqrt{\mathbf{q}'^2 + m^2} - E}, \quad (\text{E5})$$

where $E_B(k) = \sqrt{k^2 + m_B^2}$, the energy of the emitted boson, while E is the off-shell energy of the nucleon from which the boson B has been emitted:

$$E = \sqrt{(\mathbf{q}' - \mathbf{k})^2 + m^2}. \quad (\text{E6})$$

Using E as a variable, rather than $\cos \theta'$, we may re-express Eq. (E1) as

$$I(\mathbf{q}, \mathbf{k}) = \frac{1}{(2\pi)^3 k \sqrt{V_0}} \int_0^\infty q' dq' \frac{\mathcal{F}(q')}{M_{J/\psi} + i\epsilon - 2\sqrt{\mathbf{q}'^2 + m^2}} \int_{E_-}^{E_+} \frac{E dE}{M_{J/\psi} + i\epsilon - E_B(k) - \sqrt{\mathbf{q}'^2 + m^2} - E} \\ \times \int_0^{2\pi} d\varphi' T_{N\bar{N}}(\chi', E_{N\bar{N}}) U^0(\mathbf{q}', \mathbf{k}), \quad (\text{E7})$$

where we have used the relation $E dE = -k q' d \cos \theta'$ and where $\mathcal{F}(q')$ denotes the source function as given by Eq. (9). The explicit dependence on \mathbf{q} in $I(\mathbf{q}, \mathbf{k})$ comes from the χ' dependence in the half off-shell scattering matrix. The limits of integration for the E integration are

$$E_\pm = \sqrt{m^2 + (k \pm q')^2}. \quad (\text{E8})$$

The invariant mass squared of the $N\bar{N}$ pair, $s = M_{N\bar{N}}^2$, is

$$s = (\sqrt{\mathbf{q}'^2 + m^2} + \sqrt{(\mathbf{q}' - \mathbf{k})^2 + m^2})^2 - \mathbf{k}^2, \quad (\text{E9})$$

since the total momentum of this pair is $-\mathbf{k}$ and the relative energy⁵

$$E_{N\bar{N}} = \sqrt{s + \mathbf{k}^2} - \sqrt{4m^2 + \mathbf{k}^2}. \quad (\text{E10})$$

Note that in the nonrelativistic limit this expression goes to

$$E_{N\bar{N}} \approx \frac{s - 4m^2}{4m}. \quad (\text{E11})$$

At threshold $E_{N\bar{N}} = 0$, so that $s = 4m^2$ and the emitted boson reaches its maximum momentum value, i.e., $k = 979.9$ MeV/c for the photon and $k = 742.5$ MeV/c for the ω . At the other end of the spectrum, for the emitted boson $k = 0$ and $s = (M_{J/\psi} - M_B)^2$, and we point out that there is no singularity in the integral due to this value of $k = 0$.

The integral over φ' is performed numerically without difficulty and displays no singularity. In each of the other two integrations, there is the presence of a pole. In the q' integral, the pole in q' lies at $q_p = \sqrt{M_{J/\psi}^2 - 4m^2}/2 = 1231.82$ MeV, as one can write

$$\frac{1}{M_{J/\psi} - 2E(q') + i\epsilon} = -\frac{M_{J/\psi} + 2E(q')}{4(q' - q_p - i\epsilon)(q' + q_p)}. \quad (\text{E12})$$

For practical calculation of the integral (E7), it is sufficient to integrate the q' variable up to the maximum value $q_{Max} = 12 \text{ fm}^{-1}$ (2367.94 MeV).

⁵In the spirit of the Paris potential and its parametrization, the nonrelativistic approximation to this expression would read

$$E_{N\bar{N}} \approx \frac{T_{lab}}{2} \left\{ 1 - \left(\frac{T_{lab}}{8m} + \frac{k^2}{8m^2} \right) \right\} \quad \text{with} \quad T_{lab} = \frac{s - 4m^2}{2m}.$$

In Eq. (E7), there will be a pole in E at

$$E_p = M_{J/\psi} - E_B(k) - E(q'), \quad (\text{E13})$$

if $E_- \leq E_p \leq E_+$, i.e., if

$$\sqrt{(q' - k)^2 + m^2} \leq M_{J/\psi} - \sqrt{k^2 + M_B^2} - \sqrt{q'^2 + m^2} \leq \sqrt{(q' + k)^2 + m^2}. \quad (\text{E14})$$

Study of the inequalities (E14) allows us to write the integral (E7) as

$$I(\mathbf{q}, \mathbf{k}) = I_1 + I_2 + I_3, \quad (\text{E15})$$

with

$$I_1 = \int_0^{q_1} dq' \dots (\text{no pole in } q') \int_{E_-}^{E_+} dE \dots (\text{no pole in } E), \quad (\text{E16})$$

$$I_2 = \int_{q_1}^{q_2} dq' \dots (\text{no pole in } q') \int_{E_-}^{E_+} dE \dots (\text{pole in } E), \quad (\text{E17})$$

and

$$I_3 = \int_{q_2}^{q_{Max}} dq' \dots (\text{pole in } q') \int_{E_-}^{E_+} dE \dots (\text{no pole in } E). \quad (\text{E18})$$

In the above integrals, I_1 , I_2 , and I_3 the dots (...) are to be identified with the corresponding functions given in Eq. (E7). Defining

$$q^\pm = \frac{-ks \pm \sqrt{s^2(k^2 + s - 4m^2) - 4m^2k^2s}}{-2s} = \frac{k}{2} \mp \frac{1}{2} \sqrt{(s + k^2) \frac{(s - 4m^2)}{s}} \quad (\text{E19})$$

and

$$E_{N\bar{N}}^0 = \frac{M_{J/\psi}^2 - m_B^2}{4(M_{J/\psi} - m)} - m = \frac{(M_{J/\psi} - 2m)^2 - m_B^2}{4(M_{J/\psi} - m)}, \quad (\text{E20})$$

one finds for $E_{N\bar{N}} \leq E_{N\bar{N}}^0$, $q_1 = q^+$, $q_2 = q^-$ and for $E_{N\bar{N}} \geq E_{N\bar{N}}^0$, $q_1 = -q^+$, $q_2 = q^-$. For $E_{N\bar{N}} = E_{N\bar{N}}^0$, $q_1 = 0$. The boundary $E_{N\bar{N}}^0$ is equal to 172.48 MeV for the photon case and to 101.54 MeV for the ω one. Note that at the $p\bar{p}$ threshold there is no pole in the integrals over dE , and

$$I(0, \mathbf{k}) = \int_0^{q_{Max}} dq' \dots (\text{pole in } q') \int_{E_-}^{E_+} dE \dots (\text{no pole in } E). \quad (\text{E21})$$

In the numerical program for the loop calculation, the principal value integrals in E and in q' are calculated using the FORTRAN subroutine dqawce.f, a download from the quadpack-netlib website (<http://www.netlib.org/quadpack/>).

-
- [1] Facility for Antiproton and Ion Research [www.fair-center.de]
[2] D. Gotta, Precision spectroscopy of light exotic atoms, *Prog. Part. Nucl. Phys.* **52**, 133 (2004).
[3] S. Wycech, J.-P. Dedonder, and B. Loiseau, Baryonium, a common ground for atomic and high energy physics, *Hyperfine Interact.* **234**, 141 (2015).
[4] J. Z. Bai, Y. Ban, J. G. Bian, X. Cai, J. F. Chang, H. F. Chen, H. S. Chen, J. Chen, Jie Chen, J. C. Chen *et al.* (BES Collaboration), Observation of a Near-Threshold Enhancement in the $p\bar{p}$ Mass Spectrum from Radiative $J/\psi \rightarrow \gamma p\bar{p}$ Decays, *Phys. Rev. Lett.* **91**, 022001 (2003).
[5] M. Ablikim, M. N. Achasov, D. Alberto, D. J. Ambrose, F. F. An, Q. An, Z. H. An, J. Z. Bai, R. B. F. Baldini Ferroli, Y. Ban *et al.* (BESIII Collaboration), Spin-Parity Analysis of $p\bar{p}$ Threshold Structure in J/ψ and $\psi(3686)$ Radiative Decays, *Phys. Rev. Lett.* **108**, 112003 (2012).
[6] A. Datta and P. J. O'Donnell, A new state of baryonium, *Phys. Lett. B* **567**, 273 (2003).
[7] B. Loiseau and S. Wycech, Antiproton-proton channels in J/ψ decays, *Phys. Rev. C* **72**, 011001 (2005).
[8] B. El-Bennich, M. Lacombe, B. Loiseau, and S. Wycech, Paris $N\bar{N}$ potential constrained by recent antiprotonic-atom data and $\bar{n}p$ total cross sections, *Phys. Rev. C* **79**, 054001 (2009).
[9] J. Haidenbauer, U.-G. Meißner, and A. Sibirtsev, Near threshold $p\bar{p}$ enhancement in B and J/ψ decays, *Phys. Rev. D* **74**, 017501 (2006).
[10] A. Sibirtsev, J. Haidenbauer, S. Krewald, U.-G. Meißner, and A. W. Thomas, Near threshold enhancement of the $p\bar{p}$ mass spectrum in J/ψ decay, *Phys. Rev. D* **71**, 054010 (2005).
[11] X.-Y. Kang, J. Haidenbauer, and U.-G. Meißner, Near threshold $p\bar{p}$ invariant mass spectrum measured in J/ψ and ψ' decays, *Phys. Rev. D* **91**, 074003 (2015).
[12] G. Y. Chen, H. R. Dong, and J. P. Ma, Near threshold enhancement of $p\bar{p}$ system and $p\bar{p}$ elastic scattering, *Phys. Lett. B* **692**, 136 (2010).

- [13] A. I. Milstein and S. G. Salnikov, Interaction of real and virtual $p\bar{p}$ pairs in $J/\psi \rightarrow p\bar{p}\gamma(\rho,\omega)$ decays, *Nucl. Phys. A* **966**, 54 (2017).
- [14] M. Ablikim, J. Z. Bai, Y. Ban, J. G. Bian, X. Cai, H. F. Chen, H. S. Chen, H. X. Chen, J. C. Chen, Jin Chen *et al.* (BES Collaboration), Observation of a Resonance X (1835) in $J/\psi \rightarrow \gamma\pi^+\pi^-\eta'$, *Phys. Rev. Lett.* **95**, 262001 (2005).
- [15] J.-P. Dedonder, B. Loiseau, B. El-Bennich, and S. Wycech, Structure of the X (1835) baryonium, *Phys. Rev. C* **80**, 045207 (2009).
- [16] M. Ablikim, M. N. Achasov, S. Ahmed, O. Albayrak, M. Albrecht, M. Alekseev, D. J. Ambrose, A. Amoroso, F. F. An, Q. An *et al.* (BES III Collaboration), Study of $\eta(1475)$ and X(1835) in radiative J/ψ decays to $\gamma\phi$, *Phys. Rev. D* **97**, 051101 (2018).
- [17] M. Ablikim, J. Z. Bai, Y. Ban, X. Cai, H. F. Chen, H. S. Chen, H. X. Chen, J. C. Chen, Jin Chen, Y. B. Chen *et al.* (BES Collaboration), Study of J/ψ decaying to $\omega p\bar{p}$, *Eur. Phys. J. C* **53**, 15 (2008).
- [18] M. Ablikim, M. N. Achasov, O. Albayrak, D. J. Ambrose, F. F. An, Q. An, J. Z. Bai, R. Baldini Ferroli, Y. Ban, J. Becker *et al.* (BESIII Collaboration), Study of $J/\psi \rightarrow \omega p\bar{p}$ at BESIII, *Phys. Rev. D* **87**, 112004 (2013).
- [19] J. Haidenbauer, U.-G. Meißner, and A. Sibirtsev, Near threshold $p\bar{p}$ enhancement in the $J/\psi \rightarrow \omega p\bar{p}$ decay, *Phys. Lett. B* **666**, 352 (2008).
- [20] J. P. Alexander, D. G. Cassel, S. Das, R. Ehrlich, L. Fields, L. Gibbons, S. W. Gray, D. L. Hartill, B. K. Heltsley, D. L. Kreinick *et al.* (CLEO Collaboration), Study of $\Psi(2S)$ decays to $\gamma p\bar{p}$, $\pi^0 p\bar{p}$, and $\eta p\bar{p}$, and search for $p\bar{p}$ threshold enhancements, *Phys. Rev. D* **82**, 092002 (2010).
- [21] C. Patrignani, K. Agashe, G. Aielli, C. Amsler, M. Antonelli, D. M. Asner, H. Baer, Sw. Banerjee, R. M. Barnett, T. Basaglia *et al.* (Particle Data Group), Review of particle physics, *Chin. Phys. C* **40**, 100001 (2016).
- [22] M. Ablikim, M. N. Achasov, X. C. Ai, O. Albayrak, M. Albrecht, D. J. Ambrose, A. Amoroso, F. F. An, Q. An, J. Z. Bai *et al.* (BES III Collaboration), Study of $J/\psi \rightarrow p\bar{p}\phi$ at BESIII, *Phys. Rev. D* **93**, 052010 (2016).
- [23] T. Barnes, Xiaoguang Li, and W. Roberts, Meson emission model of $\Psi \rightarrow N\bar{N}m$ charmonium strong decays, *Phys. Rev. D* **81**, 034025 (2010).
- [24] J. Bolz and P. Kroll, Exclusive J/ψ and ψ' decays into baryon-antibaryon pairs, *Eur. Phys. J. C* **2**, 545 (1998).
- [25] O. Dumbrajs, R. Koch, H. Pilkuhn, G. C. Oades, H. Behrens, J. J. de Swart, and P. Kroll, Compilation of coupling constants and low energy parameters, *Nucl. Phys. B* **216**, 277 (1983).
- [26] W. Grein and P. Kroll, Two and three pion-cut contributions to nucleon-nucleon scattering, *Nucl. Phys. A* **338**, 332 (1980).
- [27] T. A. Rijken, Extended-soft-core baryon-baryon model. I. Nucleon-nucleon scattering with the ESC04 interaction, *Phys. Rev. C* **73**, 044007 (2006).
- [28] G. Penner and U. Mosel, Vector meson production and nucleon resonance analysis in a coupled-channel approach for energies $m < s < 2$ GeV. II. Photon-induced results, *Phys. Rev. C* **66**, 055212 (2002).
- [29] V. Shklyar, H. Lenske, and U. Mosel, η -meson production in the resonance-energy region, *Phys. Rev. C* **87**, 015201 (2013).
- [30] M. Benmerrouche, R. M. Davidson, and N. C. Mukhopadhyay, Problems of describing spin-3/2 baryon resonances in the effective Lagrangian theory, *Phys. Rev. C* **39**, 2339 (1989).
- [31] S.-U. Chung, Spin formalism, BNL-76975-2006-IR - Version II - (2008), updated version of the CERN Yellow Report 71-8, (1971).
- [32] G. Höhler, E. Pietarinen, I. Sabba-Stefanescu, F. Borkowski, G. G. Simon, V. H. Walther, and R. D. Wendling, Analysis of electromagnetic nucleon form factors, *Nucl. Phys. B* **114**, 505 (1976).
- [33] L.-Y. Dai, J. Haidenbauer, and U.-G. Meißner, Antinucleon-nucleon interaction at next-to-next-to-next-to leading order in chiral effective field theory, *J. High Energy Phys.* **07** (2017) 078.
- [34] M. Ablikim, J. Z. Bai, Y. Bai, Y. Ban, X. Cai, H. F. Chen, H. S. Chen, H. X. Chen, J. C. Chen, Jin Chen *et al.* (BES Collaboration), Partial wave analysis of $J/\psi \rightarrow p\bar{p}\pi^0$, *Phys. Rev. D* **80**, 052004 (2009).
- [35] I. S. Gradshteyn and I. M. Ryzhik, *Tables of Integrals, Series, and Products* (Academic Press, San Diego, CA, 1965).
- [36] J. D. Bjorken and S. D. Drell, *Relativistic Quantum Mechanics* (McGraw-Hill Inc., New York, 1964).
- [37] H. M. Pilkuhn, *The Interactions of Hadrons* (North-Holland, Amsterdam, 1967).